

Article

# Sedimentological Controls on the Reservoir Characteristics of the Mid-Triassic Tredian Formation in the Salt and Trans-Indus Surghar Ranges, Pakistan: Integration of Outcrop, Petrographic, and SEM Analyses

Kamil A. Qureshi <sup>1,2</sup>, Mohamad Arif <sup>3</sup>, Abdul Basit <sup>4</sup>, Sajjad Ahmad <sup>3</sup> , Hammad Tariq Janjuhah <sup>5,\*</sup>   
and George Kontakiotis <sup>6,\*</sup> 

<sup>1</sup> Department of Earth Sciences, COMSATS Islamabad, Abbottabad Campus, Abbottabad 22060, Pakistan; qureshika56@gmail.com

<sup>2</sup> Department of Earth & Atmospheric Sciences, University of Houston, Houston, TX 77204, USA

<sup>3</sup> Department of Geology, University of Peshawar, Peshawar 25120, Pakistan; arif\_pkpk@yahoo.com (M.A.); dr.s\_ahmed@uop.edu.pk (S.A.)

<sup>4</sup> Geological Survey of Pakistan, Quetta 87300, Pakistan; a.basitgeo@gmail.com

<sup>5</sup> Department of Geology, Shaheed Benazir Bhutto University, Sheringal, KP, 18000, Pakistan

<sup>6</sup> Department of Historical Geology-Paleontology, Faculty of Geology and Geoenvironment, School of Earth Sciences, National and Kapodistrian University of Athens, Panepistimiopolis, Zografou, 15784 Athens, Greece

\* Correspondence: hammad@sbbu.edu.pk (H.T.J.); gkontak@geol.uoa.gr (G.K.)



**Citation:** Qureshi, K.A.; Arif, M.; Basit, A.; Ahmad, S.; Janjuhah, H.T.; Kontakiotis, G. Sedimentological Controls on the Reservoir Characteristics of the Mid-Triassic Tredian Formation in the Salt and Trans-Indus Surghar Ranges, Pakistan: Integration of Outcrop, Petrographic, and SEM Analyses. *J. Mar. Sci. Eng.* **2023**, *11*, 1019. <https://doi.org/10.3390/jmse11051019>

Academic Editor: János Kovács

Received: 24 March 2023

Revised: 30 April 2023

Accepted: 8 May 2023

Published: 10 May 2023



**Copyright:** © 2023 by the authors. Licensee MDPI, Basel, Switzerland. This article is an open access article distributed under the terms and conditions of the Creative Commons Attribution (CC BY) license (<https://creativecommons.org/licenses/by/4.0/>).

**Abstract:** The current study uses an integrated lithofacies, optical microscopy, and scanning electron microscopy (SEM) analysis to investigate the sedimentary processes, depositional architecture, and reservoir rock potential of the Tredian Formation's (Mid-Triassic) mixed siliciclastic and carbonate succession in the Salt and Trans-Indus Ranges. The formation has been divided litho-stratigraphically into two components: the lower Landa Member, which consists of fine-grained sandstone and shale, and the upper Khatkiara Member, which consists of coarse-grained sandstone. Based on sedimentary structures and lithology, four distinct types of lithofacies are identified. Two lithofacies representing sandstones interbedded with shale (LF1) and thick-bedded sandstone (LF2) lithofacies suggestive of fluvio-deltaic settings are among them. Another two lithofacies of thin-bedded sandstone (LF3) and dolomite (LF4) suggest a tidal flat depositional environment, correspondingly. The petrographic examination of the Tredian sandstones indicates a lithology ranging from sub-feldspathic arenite to feldspathic arenite with moderate packing. The presence of primary calcite cement, silica cement, and iron oxide/hydroxide cements were shown by the diagenetic investigation, which was supported by SEM studies. In addition, secondary cements include ferroan-dolomite, chlorite, and illite, which is linked with chemical alteration of unstable grains. The paragenetic sequence depicts the diagenetic evolution of the Tredian sandstone from early to late diagenetic phases. The reservoir quality of the LF1 and LF4 lithofacies has been destroyed by early-stage calcite cementation, but the lithofacies LF2 and LF3 have a strong reservoir potential owing to the scarcity of calcite cement, dissolution of unstable feldspar grains, and grain fracture.

**Keywords:** mixed siliciclastic and carbonate successions; reservoir heterogeneity; lithofacies; diagenetic evolution; cementation; regression; stratigraphic correlations; calcite and silica cement types; depositional environments

## 1. Introduction

Porosity and permeability are the key factors to assess the reservoir quality of siliciclastic rocks [1,2]. The interplay of geological factors such as tectonic history, provenance, and depositional evolution determines the mineralogical composition, grain size, shape, sorting of sandstone and control the reservoir rock's original porosity and permeability [3].

However, post-burial diagenetic processes such as compaction, cementation, dissolution, and authigenic mineralization may create or reduce the porosity of reservoir rocks [4,5].

The Upper Indus Basin (Kohat–Potwar) is one of the most prolific oil and gas-bearing basins in north Pakistan (Figure 1) [6]. Since the first commercial oil discovery in 1915 from the Miocene Siwaliks sandstone, numerous wells have been drilled in the Kohat–Potwar foreland basins, targeting multiple reservoirs. These reservoir rocks are composed of mixed siliciclastic and carbonate sequences of the Eocene, Paleocene, Cretaceous, and Jurassic ages [7–10]. However, underlying Triassic sequences were penetrated in only a few wells. The Triassic rocks consist of the Mianwali Formation (limestone), Tredian Formation (sandstone), and Kingriali Formation (dolomite), which are producing reservoirs in the Kohat–Potwar region. The Mid-Triassic Tredian Formation has been drilled in Isakhel-01, Chonai-01, and Makori-01 wells in the Upper Indus Basin and its thicknesses are 91 m, 52 m, and 22 m, respectively [11,12]. The formation tops of the Tredian sandstone were marked at a depth of 3400 m, 3795 m, and 4285 m in all these respective wells. Both Isakhel-01 and Chonai-01 are abandoned exploratory wells due to mechanical failure, while Makori-01 is the only well in the Kohat Basin in which Tredian Formation is the producing reservoir [11]. However, structural complexities involving multiple detachments and the presence or absence of salt lithofacies limit the drilling to shallow reservoirs in the fold-thrust belts of western Pakistan.

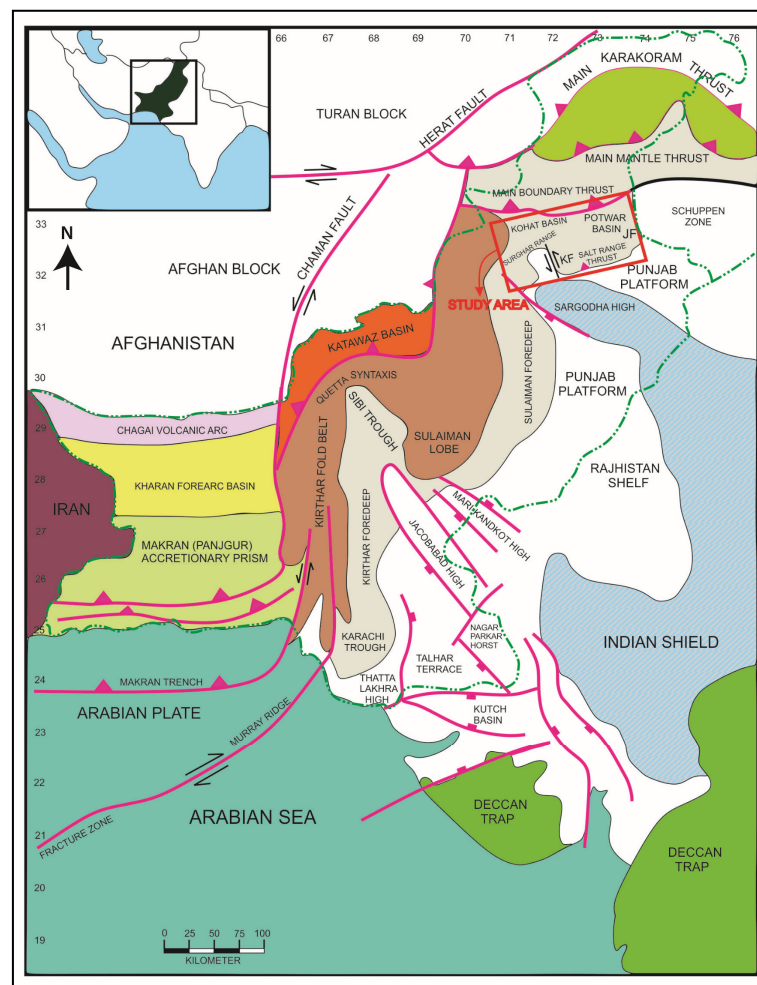


**Figure 1.** Three studied sections with their measured stratigraphic log and lateral correlation of various lithofacies of the Tredian Formation in the Salt and Trans-Indus Surghar Ranges. The measured stratigraphic sections include Landa Pasha (1), Gulakhel (2), and Nammal Nala (3), respectively. The stratigraphic thickness increases from east to west in the Landa Pasha section. Towards the west, lithofacies LF1 thickness increases and lithofacies LF2 decreases.

The Mid-Triassic Tredian Formation is well exposed in the western Salt Range and the Surghar Range. This gives scientists a unique chance to study the surface analog for predicting reservoir heterogeneity and facies variations [13,14]. Reservoir heterogeneity is caused by differences in depositional facies, diagenesis, and structural features (such as fractures or faults), and it happens on scales ranging from hundreds of meters to micrometers [14–16]. There are only a few studies conducted on the palynological and paleontological aspects of the Tredian Formation to determine its age and depositional environment [17–20]. However, details regarding vertical and lateral lithofacies variations and their diagenetic evolution are still lacking, which is important to understand the reservoir character, fluid flow, and recovery factor. The present study evaluated the reservoir quality of Tredian Formation sandstone in the three representative stratigraphic sections in the Salt and Trans-Indus Surghar Ranges (Figure 2).

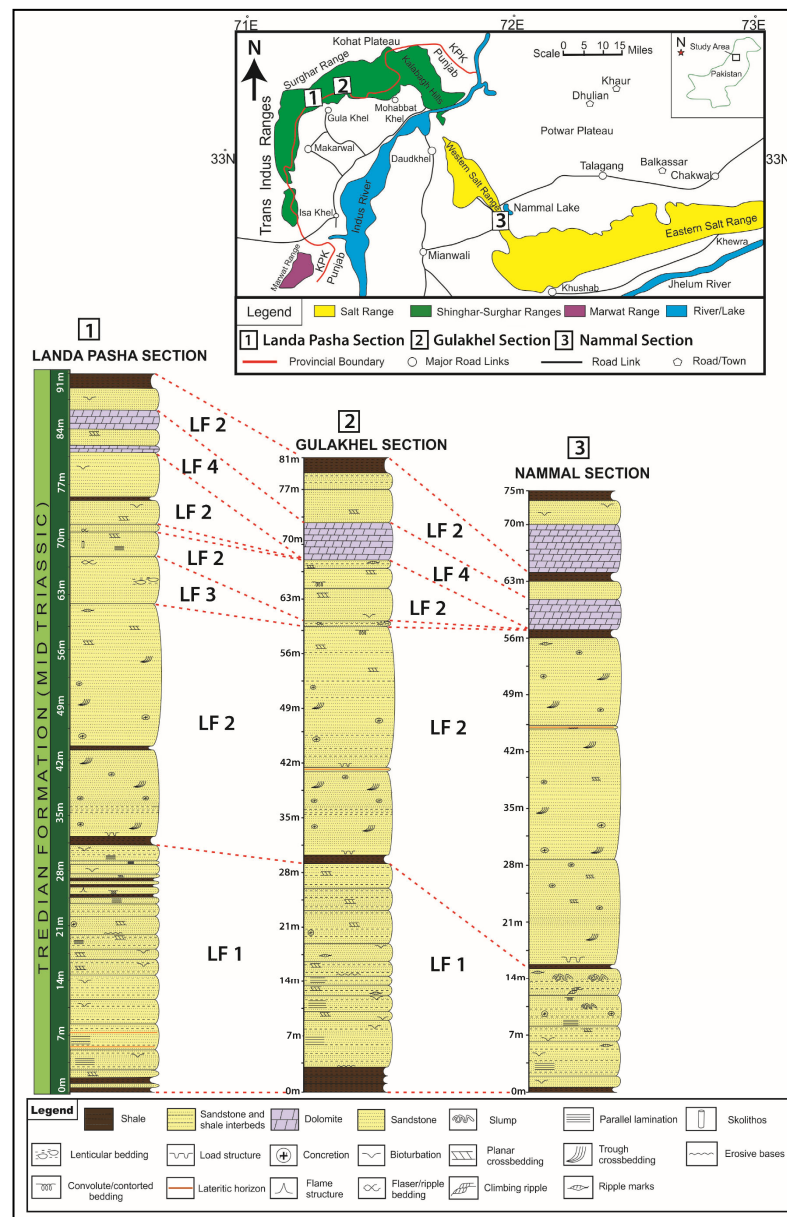


**Figure 2.** Tectono-stratigraphic framework of the western Himalayas in Pakistan. The north–south-oriented strike-slip Chaman Fault separates the western margin of the Indian plate from the Eurasian plate. The study area highlighted as red rectangle marks the foreland region as Salt and Trans-Indus Surghar Ranges and known as Main Frontal Thrust (MFT) (modified after Treloar and Izatt [21]). The numbers represent longitude and latitude, correspondingly. JF: Jhelum Fault, KF: Kalabagh Fault.

More explicitly, the current study aims to: (1) carry out lithofacies interpretation along with their vertical and lateral variations, (2) present a petrographic characterization of the Tredian Formation sandstone, (3) determine the extent and significance of diagenetic processes and its influence on reservoir quality using optical and scanning electron microscopy (SEM), and (4) provide an integrated depositional model.

## 2. Geological Framework

The Indo–Asia collision created the ~2500-kilometer-long seismically active Himalayan Mountain belt (55 Ma) [22]. The main frontal thrust (MFT) marks the southern boundary of this collisional zone and is represented by the Salt and Trans-Indus Ranges [23–25] (Figure 1). In comparison with the eastern and central Himalayas, MFT is a more than 100 km wide zone in the western Himalayas in Pakistan with a low degree of cross-sectional taper, resulting in the opening of wide basins, i.e., the Kohat and Potwar Basins [26,27]. The Salt Range has been subdivided into the eastern, central, and western sections, respectively [25,26]. The eastern termination of the Salt Range is the Jhelum Fault (left-lateral strike-slip), whereas the western termination is marked by the Kalabagh Fault (right-lateral strike-slip) [27] (Figure 1). The Salt Range Thrust (SRT) marks the leading edge of the Potwar Plateau. The sinuous shape of the Trans-Indus Ranges (TIR) demarcates the deformational front of the Kohat Basin in North Pakistan [25]. The TIR comprises the Surghar Range, the Shinghar Range, the Marwat–Khisor Ranges, the Manzai Range, and the Sheikh Badin Hills. The Surghar Range (SR) marks the eastern extremity of the Trans-Indus Ranges [28,29] (Figure 1).

Both the Salt and Trans-Indus Surghar Ranges have Triassic rocks cropping out roughly parallel to the Salt Range Thrust [30]. These successions are well exposed in different gorges, among which the Landa Pasha (Surghar Range), Gulakhel (Surghar Range), and Nammal Gorge sections (Western Salt Range) were focused during this work (Figure 2). The sedimentary successions of the Salt and Trans-Indus Surghar Ranges reflect the depositional environments of the Gondwana shelf. The depositional sites were probably located at 30° S [30,31]. The Tethyan Ocean was receiving siliciclastic sediments from the Indian subcontinent [7]. Exposed rocks in the Western Salt Range extend from the Precambrian (Salt Range Formation) to the Eocene (Sakessar Limestone). The Salt Range Thrust reveals Precambrian to Recent rocks. The Salt Range Formation represents the Precambrian age and is overlain by rocks of the Jhelum Group (Cambrian). The Permian-Eocene stratigraphic successions are well exposed in the study sections [32]. Exposed rocks in the Surghar Range show ages from the Late Permian (Wargal Formation) to Miocene (Chinji Formation). The generalized stratigraphy of the Western Salt Range (Nammal Gorge) and the Trans-Indus Surghar Range (Landa Pasha and Gulakhel sections) is shown in Figure 3.

The Triassic succession includes the Mianwali, Tredian, and Kingriali formations. The Triassic rocks have a disconformable lower contact (Permo-Triassic; P-T boundary) with rocks of the Zaluch Group, while upper contact with the Jurassic Datta Formation is conformable (Figure 3). The P-T boundary represents the great Permian extinction that occurred at about 252 Ma, during which 96% of marine species and 70% of terrestrial vertebrates became extinct [32–35]. The principal lithology of the Tredian Formation is sandstone with shale and some dolomite (Figure 2). It marks conformable contacts with the underlying Mianwali Formation and the overlying Kingriali Dolomite [7] (Figure 3). No fossils have been reported so far; however, some poorly preserved plant remains were observed by Balme [36–38].

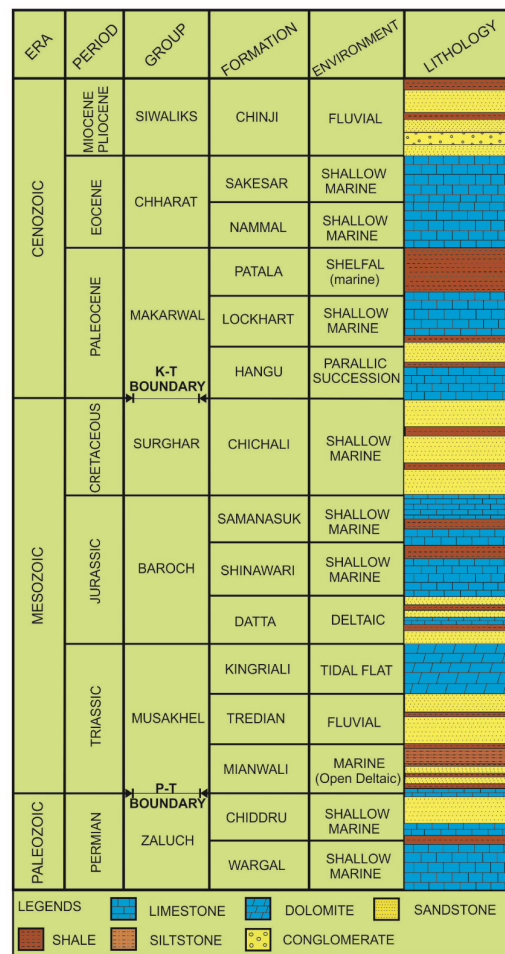


**Figure 3.** A generalized stratigraphic column in the Nammal Nala, Landa Pasha, and Gulakhel section in the Salt and Trans-Indus Surghar Ranges after Shah [7]. The rocks older than Permian Wargal Formation are missing in all these sections.

### 3. Materials and Methods

A detailed geological field trip was carried out to the Nammal Nala section (32°40'3.41" N, 71°47'9.24" E) in the western Salt Range and the Landa Pasha (32°58'0.00" N, 71°12'0.00" E) and Gulakhel sections in the Surghar Ranges, with the help of available geological maps [30], to record all pertinent field data (Figure 2). All stratigraphic sections were logged and measured with the help of a measuring tape. The measured thicknesses of the Tredian Formation at the Nammal Nala section are 75 m, the Gulakhel section is 81 m, and the Landa Pasha section is 91 m (Figure 2). A total of 46 samples were collected for petrographic analysis from the Landa Pasha section which represents a complete stratigraphic section. A 2 m sampling interval was chosen to cover all details of lithological variations. An outcrop-based lithofacies description was made using field observations, which included sedimentary structures, lithological variation, bedding, thickness, nature of contact, texture, color, fauna, and bioturbation.

After fieldwork, 35 representative rock samples were processed for thin section preparation in the rock cutting laboratory at the Hydrocarbon Development Institute of Pakistan (HDIP) for petrographic analysis. After cutting chips, casting resin and blue dye were used to impregnate samples, which determine the visual porosity percentage of the analyzed samples. Moreover, a chip was mounted on a slide made of thin glass with the help of petro-epoxy for the preparation of thin sections [39,40]. Detailed petrographic analysis was performed under the polarizing microscope available at the Petrography Laboratory of the Department of Earth Sciences, COMSATS Institute of Information Technology, Abbotabad campus, Pakistan. The SEM and EDX analyses of ten representative samples were

performed to distinguish between primary and authigenic minerals. This investigation also helped in evaluating the effect of diagenesis on the Tredian sandstone reservoir potential. The SEM analyses were performed at the Centralized Resource Laboratory (CRL), Department of Physics, University of Peshawar, under the JEOL JSM-5910 Model SEM fitted with an Energy Dispersive X-ray Micro-analyzer (EDAX).

#### 4. Results

##### 4.1. Lithofacies Description

Four lithofacies have been identified in the Tredian Formation exposed in the studied sections by utilizing various sedimentological aspects. They are characterized as fluvio-deltaic and tidal flat lithofacies. A summary of all of them is provided in Table 1.

**Table 1.** Details of the lithofacies of the Tredian Formation along with their observed sedimentary structures, description, and interpretation in all the studied sections.

Lithofacies	Sub-Lithofacies/Facies	Description	Interpretation
Lithofacies-1 (LF-1) Sandstone interbedded with shale lithofacies	Cross-bedded, parallel laminated, slumped, rippled, bioturbated sandstone facies	Medium-to-coarse grain, moderate-to-poor sorting, medium-to-thick-bedded sandstone, interbedded with carbonaceous black shales black. Commonly found sedimentary structures are cross bedding, parallel lamination, slump structures, bioturbation, symmetrical and asymmetrical ripples, flame structures, and channelized beds	The sandstone is deposited in distributary channels/channel margins of delta plain settings whereas the shale is deposited in low-energy settings of floodplain and interdistributary bay or marshes
Lithofacies-2 (LF-2) Thick bedded sandstone lithofacies	Planar cross-bedded, trough cross-bedded, rippled sandstone facies	Thick-bedded coarse-grain sandstone with planar cross bedding, trough cross bedding, ripple marks, basal erosional surface, and load marks. Pebbly bases of the beds were commonly observed. Well-developed channels are also common. Inter-bedded shale is dark greenish grey to black in color containing thin lamination of sand	The deposition of sandstone took place during high fluvial discharge in fluvial channel environment during active delta progradation, whereas the associated shale shows the deposition along the channel margins or levees
Lithofacies-3 (LF-3) Thin-bedded sandstone lithofacies	Parallel-laminated and ripple-laminated sandstone facies	Thin-bedded, greenish grey, medium-to-fine-grain sandstone. Commonly observed sedimentary structures are parallel and ripple lamination. Flaser and lenticular bedding are also common	Deposited in sand dominated delta front or tidal flats where fluctuation in sediment supply is common
Lithofacies-4 (LF-4) Dolomite lithofacies		Medium-bedded yellowish brown dolomite. The dolomite is hard, compact, and brecciated and has laterally pinching channels. The lower part is sandy dolomite, whereas the upper part is pure dolomite.	Deposited during fluctuating depositional condition in shoreface

##### 4.1.1. Fluvio-Deltaic Lithofacies

###### 1. Sandstone Interbedded with shale lithofacies (LF1)

This lithofacies is present at the base and represents the Landa Member of the Tredian Formation, which is 31 m thick in the Landa Pasha Section, 29 m thick in the Gulakhel Section, and 15 m thick in the Nammal Section, respectively (Figure 2). It can be further subdivided into five sub-lithofacies based on diagnostic sedimentary characteristics (Table 1). It is predominantly composed of medium- to coarse-grained, moderately to poorly sorted, orange/yellow to maroon-colored, medium- to thickly bedded, hard, and compact sand-

stone interbedded with dark grey to black carbonaceous shale (Figure 4). Scattered pebbles can also be seen in some places. The ratio of sandstone to shale is 3:1. The pisolitic bed at the base of this lithofacies marks the conformable contact between the Mianwali and Tredian Formations. The most commonly observed sedimentary structures are parallel lamination, cross-bedding, slumps, ripple marks, convoluted or contorted bedding, flame structures, bioturbation, and iron concretions (Figure 4c–j). The large planar tabular cross-beds have a thickness varying from 8 to 14 cm. Slumps are observed only in the Nammal Nala section and were not encountered in the other two studied sections. Bioturbation is also very common (Figure 4k). In places, well-developed channels are present and show lateral pinching (Figure 4l).

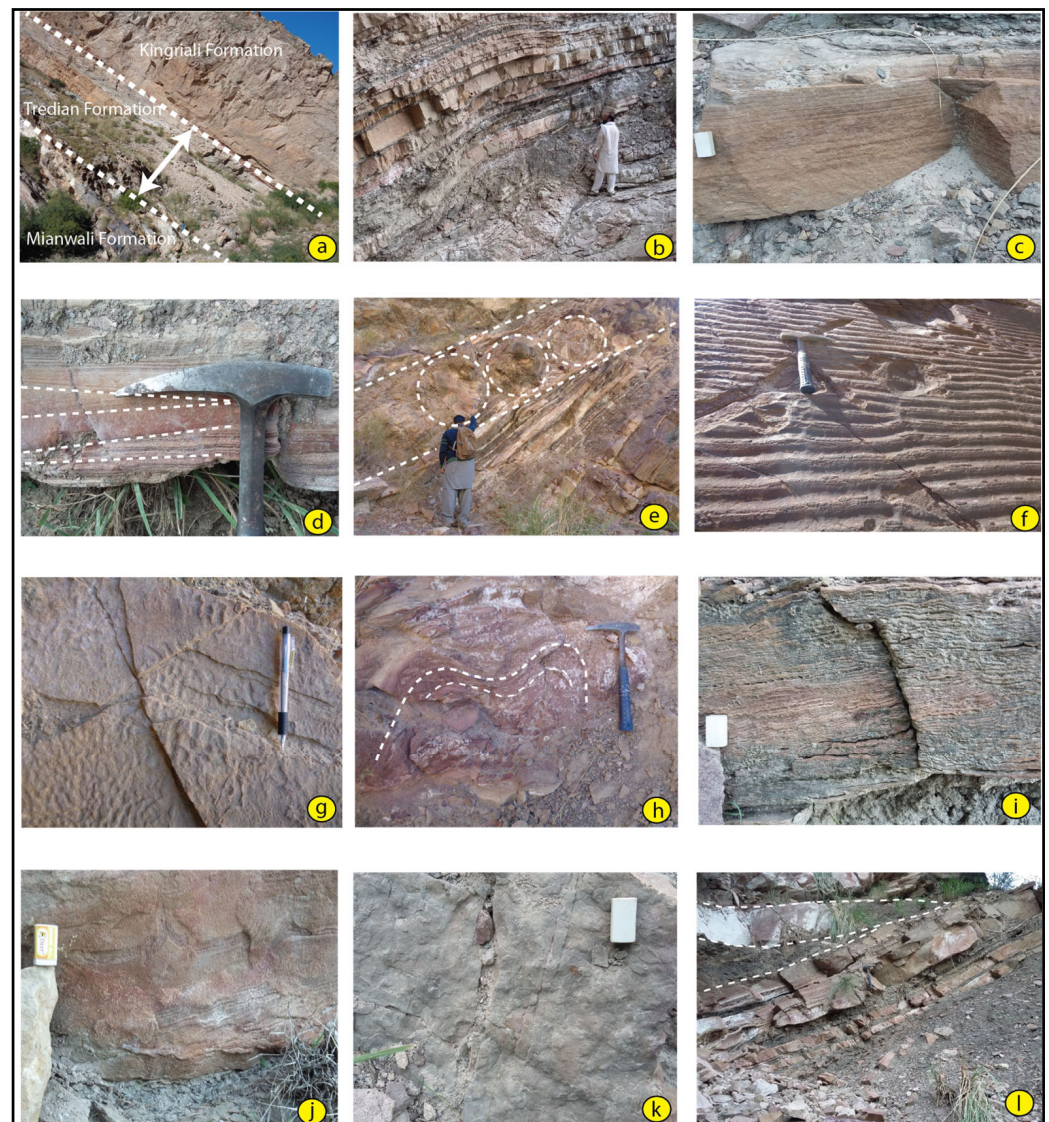


**Figure 4.** Field photographs showing various sedimentological features of Tredian Formation. (a) Outcrop exposure of Tredian Formation in Nammal Section with upper and lower conformable contacts. (b) Outcrop exposure of sandstone interbedded with shale lithofacies (LF-1). (c) Field photograph of parallel laminated medium bedded sandstone lithofacies. (d) Field photograph of cross-bedded sandstone lithofacies. (e) Field photograph showing the slumped facies of LF-1. (f) Symmetrical ripples. (g) Field photograph showing asymmetric ripples. (h) Convoluted bedding in the slumped facies of LF-1. (i) Contorted bedding. (j) Flame structures in LF-1. (k) Bioturbated sandstone facies of LF-1. (l) Well-developed channels and their lateral pinching.

## 2. Thick-Bedded Sandstone Lithofacies (LF2)

This lithofacies overlies the LF1 of the Tredian Formation and is predominantly comprised of light gray to whitish-colored, coarse-grain, thick-bedded sandstone, and carbonaceous shale (Figure 5a). The beds also have pebbly bases. The shale units are dark greenish gray to black, carbonaceous, and contain thin laminae of sand. Black carbonaceous shale marks the contact between LF1 and LF2 (Figure 5b). Lithofacies LF2 are approximately 31 m thick in the Landa Pasha and Gulakhel sections and 41 m thick in the Nammal Nala section (Figure 2). The sandstone-to-carbonaceous shale ratio is 9:1. The most commonly observed sedimentary structures are planar tabular cross-bedding, trough cross-bedding, erosional basal surfaces, and load structures. Ripple marks are commonly seen at the top of lithofacies, whereas trough and planar tabular cross bedding can be found throughout (Figure 5c–e). Syn-depositional features such as load structures are present at the base of this lithofacies. Well-developed channels are also present in lithofacies LF2 (Figure 5f).

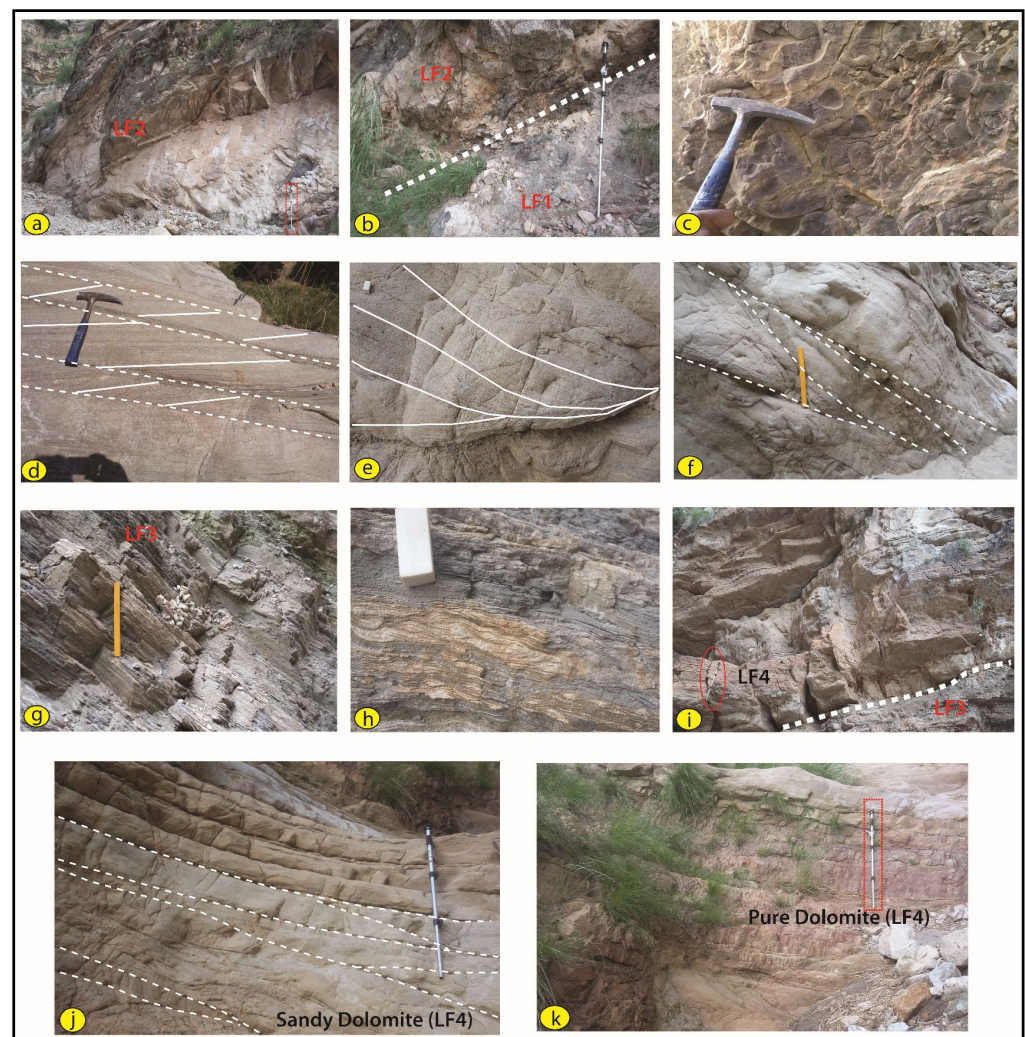


**Figure 5.** Field photographs of various sedimentological features of Tredian Formation lithofacies. (a) Channelized sandstone of LF2 (the red rectangle highlight the Jacob Staff for scale). (b) Black carbonaceous shales mark the contact between LF1 and LF2. (c) Pebbly bases in LF2. (d,e) Planar and trough cross-bedded sandstone facies LF-2. (f) Thick-bedded sandstone lithofacies LF2 with channel pinching. (g) Thin-bedded sandstone with interbedded shale lithofacies (LF-3). (h) Rippled sandstone facies with flaser and lenticular bedding in LF3. (i) Thick-bedded dolomitic lithofacies LF4 on top of LF3. (j) Sandy dolomite lithofacies with laterally pinching channels. (k) Top unit of pure dolomitic lithofacies LF4.

#### 4.1.2. Tidal Flat Lithofacies

##### 1. Thin-Bedded Sandstone Lithofacies (LF3)

This lithofacies overlies LF2 in the Landa Pasha section and the Gulakhel section, whereas it is altogether missing in the Nammal Nala section (Figure 2). The measured thickness of LF3 in the Gulakhel and Landa Pasha sections is 1 m and 6 m, respectively. The ripple sandstone of LF2 grades upward into flaser bedded LF3 lithofacies. It comprises medium-to-fine-grained, greenish gray to whitish or brownish, moderately to well-sorted, and thin-bedded sandstone (Figure 5g). Sand lenses are 1 to 3 cm thick and show ripple laminations (Figure 5h). Further towards the top, the flaser and lenticular bedding are replaced by parallel lamination.

##### 2. Dolomite Lithofacies (LF4)

This lithofacies overlies the thin-bedded sandstone lithofacies LF3 and contains sandy dolomite (Figure 5i). Dolomite is yellowish-brown to pinkish in color. The total thickness of this unit is 3 m in the Landa Pasha section, 5 m in the Gulakhel section, and 10 m in the Nammal section, respectively (Figure 2). The dolomite is hard, compact, brecciated, and has laterally pinching channels (Figure 5j). The lower part of the lithofacies is sandy dolomite, while the upper part is pure dolomite (Figure 5k).

#### 4.2. Petrographic Analysis

The petrographic analysis of sandstone samples collected from the Tredian Formation revealed that it comprises fine-to-coarse framework grains and cement. Based on the model composition of Pettijohn [41], the sandstone is classified as sub-feldspathic arenite to feldspathic arenite. The predominant mineralogical constituents include quartz, feldspar, accessory minerals, mica, and lithic fragments. Most of the grains are sub-rounded and sub-angular to angular. The grains packing and sorting are moderate. Texturally, the sandstone is sub-mature to mature, whereas compositional maturity varies from sub-mature to immature. The most predominant constituent framework grain in the Tredian Formation is quartz, which has an average abundance of 49.4% (Table 2).

Grains shape is mostly sub-spherical with angular to sub-rounded outlines. Some well-rounded quartz grains are also present, which shows long distances of transport (Figure 6a). A clay rim was observed in a few quartz grains (Figure 6b). The grain contact can be pointed, long, concavo-convex, or suture-like (Figure 6b). Some fractured quartz grains are also present, but they are empty and not filled with cement. Some clean grains have quartz cement present as overgrowth (Figure 6a).

Medium-grained feldspar is the second most abundant mineral in the Tredian Formation, which exists in both plagioclase and K-feldspar forms with an average abundance of 14.3% (Table 2) (Figure 6c). Plagioclase, on the other hand, has the lowest concentration. The grain shape is sub-spherical to prismatic with sub-angular to sub-rounded outlines. Some of the samples have feldspar grains that are partially or completely altered to clay minerals (Figure 6d,e). Lithic fragments include some minor fossils and siltstone lithics. The proportion of fossil fragments in the sandstone studied is less than 1% (Figure 6f). Calcite cement mostly replaces fossil fragments, while the margins of some fragments are altered by reacting with cementing fluids. Muscovite occurs in significant quantity in the studied thin sections. Its average abundance is 5.3%; however, in a few thin sections, it ranges up to 29.6%.

It mostly occurs as long individual flakes (Figure 6g). Biotite is present in trace amounts in the samples. They show clay alteration in some places. Its average abundance is 0.6%. The modal abundance of the accessory minerals in the Tredian sandstone is 0.85% (a trace amount), including the grains of tourmaline, rutile, and zircon (Figure 6h,i).

**Table 2.** Percentage modal proportions of framework elements in the Tredian Formation. Qt: Quartz total; Qm: Quartz monocrystalline; Qp: Quartz polycrystalline; Al.Feld: Alkali Feldspar; PlG: Plagioclase; Poros: Porosity; Musc: Muscovite; Biot: Biotite; Ceme: Cement. Accessory minerals include zircon, rutile, etc.

SN	S#	Quartz			Feldspar		Lithoc	Pores	Musc	Biot	Ceme	Ore	Accessort Minerals	Classification
		Qt	Qm	Qp	AlFeld	PlG								Pettijohn
1	T1	48	48	0	10	1	0	0	4	1	35	0	1	Sub-Arkose
2	T2	46	46	0	8	0.5	0	0	3	0.5	42	0	0	Sub-Arkose
3	T3	40	39.8	0.2	9	2.6	0	2	5.5	1	29.5	10	0.4	Sub-Arkose
4	T4	65	65	0	9	3	0	2.5	2.5	1	10	5	2	Sub-Arkose
5	T5	51	50.5	0.5	14	0.5	0.5	0	2	0	28	2.5	1.5	Sub-Arkose
6	T6	33	33	0	18	1.5	0	2	4	0	39	2	0.5	Arkose
7	T8	60	60	0	11	2	0.4	3	8	0.6	8	6	1	Sub-Arkose
8	T9	58	58	0	7	1.2	0	1	4	2	22	4	0.8	Sub-Arkose
9	T11	44	43	1	14.5	0.5	0	1.5	10.5	0.6	19	9	0.4	Arkose
10	T12	60	60	0	17	3	0	3	1.6	1	1	12	1.4	Arkose
11	T14	58	58	0	18	1	1	4	5	2	4	5	2	Sub-Arkose
12	T16	56	55.5	0.5	15	3	0	10	1.5	0	6	8	0.5	Sub-Arkose
13	T17	47	47	0	20	1.5	0.5	1	0.6	1.5	16	7	1	Arkose
14	T18	52	52	0	22	2.5	0	6	0.5	0.6	8	4.5	2	Arkose
15	T19	35	35	1.5	11	2	0	1	1	0.5	44	4	0.5	Arkose
16	T20	84	84	0	7	0.3	0	4	0	1	2	0.7	1	Sub-Arkose
17	T21	16	16	0	8	0.8	0	0	0	0	66	9	0.2	Arkose
18	T22	14	14	0	9	1	0	6	0	0	64	6	0	Arkose
19	T24	60	60	0	19	1.5	0	4	4.5	0	9	1	1	Arkose
20	T25	38	36	2	14	2	0	0	3	1	36	5	1	Arkose
21	NT5	55	55	0	24	2.4	0	3	8.5	0.5	2	3.6	1	Arkose
22	NT6	66	65.2	0.8	12	0.5	0	2	12.5	0	6	1	0	Sub-Arkose
23	NT7	36	36	0	10	2	0	0	20	0	27	5	0	Sub-Arkose
24	NT9	32	31	1	13.5	1.9	0	0	13.4	1	29	7	2.2	Arkose
25	NT10	30	30	0	11	1.5	0	0	2.8	0.2	45	8	1.5	Arkose
26	NT12	78	78	0	7	1.8	0	13	0	0	0	0	0.2	Sub-Arkose
27	NT13	71	70.5	0.5	7	0.5	0	5	0	0	15	1	0.5	Sub-Arkose
28	NT14	80	80	0	5	1.2	0	8	0	0	5	0	0.8	Sub-Arkose
29	NT17	19	19	0	20	1	0	0	29.6	2	28	0	0.4	Arkose

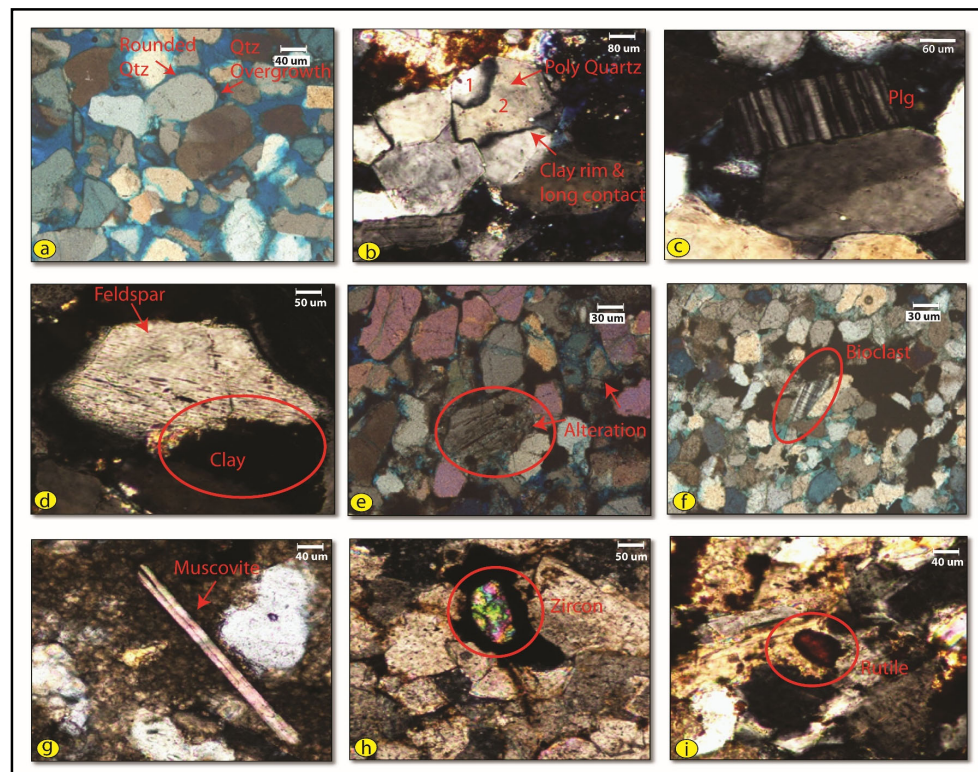


**Figure 6.** Petrographic analysis of framework grains. (a) Rounded quartz grains with quartz overgrowth in LF2. (b) Polycrystalline quartz with clay rim at grain boundaries and long grain contact in LF1. (c) Plagioclase grain with twinning in LF1. (d) Feldspar grain with clay alteration at the boundary and some replacement by cement in LF3. (e) Feldspar grain showing partial/complete alteration to clay in LF2. (f) Bioclast with some clay present at the boundary in LF2. (g) Long muscovite flake in LF1. (h) Accessory mineral zircon with clay rim at the boundary in LF1, and (i) rutile grain embedded in calcite cement in LF1.

### 4.3. Diagenesis of the Tredian Sandstone

#### 4.3.1. Compaction

Compaction is considered the main factor affecting the reservoir as well as other physical properties of the Tredian Formation sandstone. The precipitation of early calcite cement marks the end of further compaction. The following types of grain packing explain the degree of compaction observed in Tredian Formation sandstone (Figure 7a–f). The depositional settings of various interpreted lithofacies are also described.

- (a) Loosely packed grains: Loose packing of grains was observed at the basal part of the Tredian Formation, where precipitation of calcite cement ceased the further compaction of grains. The floating grains are observed with point and long-line contact, which also refers to the loose packing of grains (Figure 7a).
- (b) Closely packed grains: This type of packing includes moderate-to-strong packing of grains. Line/long contact of grains is observed, where the packing is moderate, whereas concave-convex contact with pressure solutions refers to the strong packing of grains (Figure 7b).
- (c) Directionally oriented packed grains: Flake mineral grains such as micas were mainly characterized by directional arrangement due to the pressure of overlying strata (Figure 7c).
- (d) Plastic grains deformed by extrusion: The plastic grains such as micas and chlorites were observed to be bent or broken where the compaction was strong (Figure 7d).

- (e) Rigid grains crushed by extrusion: Rigid grains such as feldspar and quartz are broken, forming micro-fractures, when the compaction further increases with increase in burial depth (Figure 7e).
- (f) Chemically compacted fabric: Pressure-induced dissolution along the contacts of quartz grains provided the silica cement, which filled the pore spaces and resulted in the reduction of inter-granular porosity. This chemical compaction is observed mostly at the upper part of the Tredian Formation (Figure 7f).

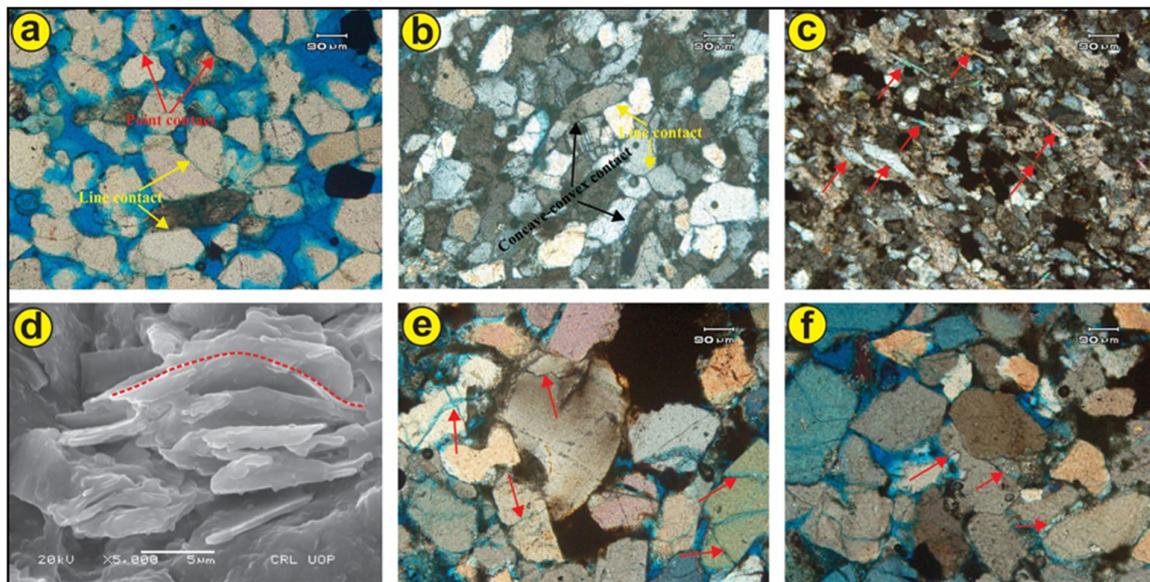


**Figure 7.** Photomicrographs of Tredian sandstone showing various degrees of compaction and associated features. (a) Loosely packed grains with pointed and long contact. (b) Closely packed grains with long and concavo-convex contact between the grains showing moderate-to-strong degree of compaction, respectively. (c) Directionally oriented packed grains (red arrows) showing directional arrangement due to the pressure of overlying strata. (d) Bent grains of chlorite showing plastic grain deformation by extrusion. (e) Fractured grains in quartz and feldspar showing micro-fractures. (f) Chemically compacted fabric with pressure-induced dissolution (red arrows) along the contacts of quartz grains.

#### 4.3.2. Cementation

After compaction, cementation is another important contributing factor that affects the reservoir quality of Tredian Formation sandstone by reducing the porosity and permeability. Precipitation of various types of cement (Figure 8a–d) reduced the pore spaces and the connectivity of pore throats, hence affecting reservoir quality. Petrographic studies and SEM analyses have revealed the occurrence of the following types of cement described below.

Calcite cement is the most dominant type of cement observed in Tredian Formation sandstone and occurs in both well-developed poikilotopic (Figure 8a) and fine-grained micritic forms (Figure 8b). The following two stages of calcite cementation are distinguishable based on distribution and texture: (a) Early diagenetic calcite cement developed between the floating framework grains in poikilotopic form at the basal part of the Tredian Formation (LF1); (b) Late diagenetic calcite cement was found in some samples from the Khatkiara Member. The late-stage fine-grain calcite cement has precipitated in the inter-granular pore spaces (LF2). Siliceous cementation in the form of quartz overgrowth was commonly observed in the samples taken from the Khatkiara Member of the Tredian Formation (LF2). The presence of quartz overgrowth indicates the availability of sufficient silica, a medium for its transport, and a clean surface of grains for its precipitation (Figure 8c). The early diagenetic calcite cementation in the Landa Member halted the silica precipitation in the form of quartz overgrowth; hence, quartz overgrowth was not observed in the Landa

Member of the Tredian Formation (Figure 8a). All the studied samples of the Tredian sandstone contain a significant amount of ferruginous cement (Figure 8d). It decreases the amount of secondary porosity by replacing the initial cement through dissolution. It is present both as pore-filling and grain-occluding phases.

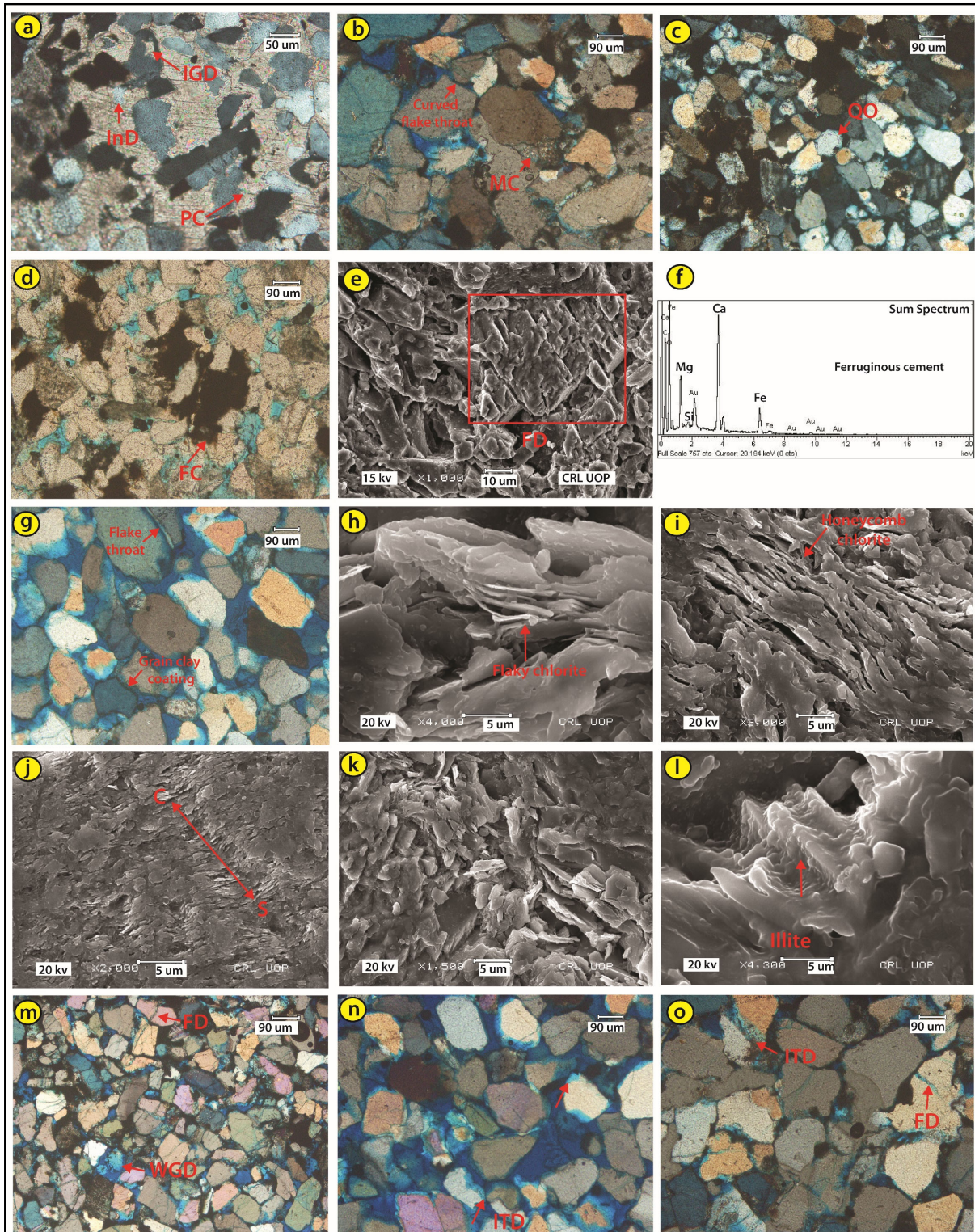


**Figure 8.** Photomicrograph showing various diagenetic features of Tredian sandstone. (a) Poikilotropic calcite cement (PC), interstitial dissolution (InD), and Intra-granular dissolution (IGD) in quartz grains.

(b) Connectivity between the pores through curved flake throat and micritic calcite cement (MC). (c) Strongly compacted grains with quartz overgrowth (QO). (d) Ferruginous cement (FC) as cementing material. (e) SEM image showing ferroan dolomite (FD). (f) EDX spectra showing ferruginous cement. (g) Pores connectivity through flake throat and clay coating around the grains. (h) SEM image showing flaky/rosettes chlorite. (i) SEM image showing honeycomb/leafy chlorite. (j) SEM image showing chloritization of smectite. (k) Small and thin platelets of mixed-layer illite-chlorite occurring as void filling. (l) SEM image showing early diagenetic illite. (m) Fracture dissolution (FD) and whole-grain dissolution (WGD). (n) Inter-granular dissolution (ITD) and connectivity of pores through neck throat. (o) Fracture dissolution and inter-granular dissolution.

Other types of cement include Ferroan dolomite which occurs in most of the samples as well-developed authigenic crystals, as identified petrographically and confirmed through SEM/EDX analysis (Figure 8e,f). The dolomite rhombs are fine grain in size and occur during the grain-replacing and pore-occluding phases. The ferroan dolomite in sandstone represents reducing and alkaline pore water conditions [42]. Chlorite is another commonly observed cement type that exists in both Rosettes (Figure 8h) and honeycomb (Figure 8i) as morphological forms. Chlorite occurs both as a grain coating and as pore filling (Figure 8g). Alteration of feldspars, direct precipitation of chlorite from pore fluids, and chloritization of other clay minerals are the most likely sources of chlorite formation [34,43]. Chloritization of smectite is observed through SEM analysis (Figure 8j). Chlorite with an irregular morphology is sometimes mixed with illite and forms a mixed layer of illite and chlorite. Small and thin platelets of illite-chlorite also occur as void filling (Figure 8k). Two types of chlorites have been recognized in studied samples: (a) Early diagenetic chlorite: In most of the samples, it lies perpendicular to the detrital grain surfaces suggesting their formation during early diagenesis [34,44]; (b) Late-stage burial diagenetic chlorite: The chlorite presents as pore-filling forms during burial diagenesis. Illite is present in the studied samples with a hair-like fibrous and ribbon crystal habit (Figure 8l). The typical illite is lath-like and represents kaolinite as its precursor. In the studied sandstone samples, illite occurs as pore-filling material. A markedly greater abundance of illite in the vicinity of altered detrital grains of feldspar strongly suggests the formation of illite by feldspar alteration. Illite is an exclusively burial diagenetic mineral, and its formation requires the availability of potassium and a temperature exceeding 70 °C [45].

#### 4.3.3. Dissolution

Dissolution is a main contributing factor in enhancing the reservoir character of sandstone. Following are the different types of dissolution observed in the sandstone of the Tredian Formation: (a) Intra-granular dissolution is observed inside the grains, which have been dissolved by acidic fluids. The dissolved part of the grain either exists in the shape of spots or honeycomb shape (Figure 8a,f); (b) Whole-grain dissolution was common in some grains forming moldic pores (Figure 8f,m); (c) Dissolution along weak planes was commonly observed along the cleavage planes, cracks, and fractures of feldspar grains (Figure 8f); (d) Inter-granular dissolution is a kind of irregular dissolution that is observed along the edges of some soluble grains, such as feldspar and lithic grains (Figure 8n,o); (e) Interstitial dissolution is also observed, in which interstitial material, such as calcite cement, has been dissolved, forming interstitial pores (Figure 8a).

## 5. Discussion

### 5.1. Lithofacies Depositional Environment

#### 5.1.1. LF-1 Interpretation

The presence of features such as ripple marks, planar cross-bedding, parallel lamination, and bioturbation indicates deposition of this lithofacies in distributary channels and inter-distributary bays, which are the principal components of a delta plain [46–48]. The presence of scattered pebbles also supports the deposition in delta plain settings [49]. The cross bedding is the indication of deposition under unidirectional flow, which is mostly associated with fluvial channels or distributary channels in a delta plain setting [50–52].

Parallel laminated sandstones represent deposition in upper-flow regime conditions [53,54]. This lithofacies has a close association with the shoreline/shoreface setting; however, the presence of slumps, which is uncommon in a shoreline environment, describes it as a delta plain facies [55]. The presence of wave ripples indicates that this lithofacies was also affected by shoreline/beach action; however, the presence of erosive bases, channel morphology, channel lag, cross-bedding, planar lamination, bioturbation, and slump structures supports deposition in distributary channels/channels or channel margins of delta plain settings, whereas the shale was deposited in low-energy settings of flood plains and inter-distributary bay/marshes [56].

#### 5.1.2. LF-2 Interpretation

The well-developed channels with erosive and pebbly bases, load structures, large cross-bed sets (trough and planar), and coarse grain size in LF2 indicate deposition during high-energy tractional flows [55,57]. The migration of three-dimensional large bedforms results in trough cross bedding, which commonly occurs in the channel belt facies in upper and middle delta plain areas [52,58,59]. Hence, channel morphology, sedimentary structures, and coarse grain size help interpret its deposition in a delta plain or fluvial channel environment during active delta progradation. Deposition of the sandstone took place during high fluvial discharge. The associated carbonaceous shale/clay shows deposition along the channel levee/margin [60].

#### 5.1.3. LF-3 Interpretation

This thin-bedded lithofacies has developed over the thick-bedded, channelized LF2 lithofacies. The presence of abundant ripples shows deposition in a coastal environment [61–63]. The lithofacies have flaser and lenticular bedding, reflecting fluctuating depositional conditions [64]. The rippled sands and mud drapes are associated with the current activity of sand-dominated tidal flats, and as the abundance of mud decreases, the bedding changes from lenticular to flaser type [65]. Moreover, flaser and lenticular bedding are common in tidal flats and in the delta front environment, where fluctuation in sediment supply is common [66]. It may also be interpreted to represent deposition in a tidal setting, i.e., tidal flats and tidal channels [67]. Its position above the fluvial lithofacies (LF2) and below the dolomitic lithofacies (LF4) shows the onset of marine conditions. Hence, it is concluded that this lithofacies was deposited in the tidal flat setting.

#### 5.1.4. LF-4 Interpretation

The presence of dolomite marks the onset of marine conditions. Lithology grades from pure fluvial sand through sandy dolomite to pure dolomite and further up into the thick dolomite of the Kingriali Formation. This change in lithology marks the change in environmental conditions, i.e., the dominant siliciclastic system of the Mid-Triassic Tredian Formation was finally changed into the carbonate system of the Upper Triassic Kingriali Dolomite [68,69]. However, there is no obvious clue of any tectonic activity for this change of the system. The transgressive sequence of this lithofacies marks the delta abandonment, as also documented in the Rhone and Niger deltas [51,70], as well as the Mississippi Delta [71]. The process of transgression takes place due to delta switching after the abandonment of the delta, with components of reworking of shoreface retreat and submergence [72]. The presence of ripple marks and dolomite indicates fluctuating depositional conditions and suggests shallow beach or near-shore depositional settings due to reworked sands of retreating shorefaces [49,64].

### 5.2. Depositional Settings

The dominant characteristics like facies association, composition, and distribution of the Tredian sandstone suggest its deposition in a fluvio-deltaic environment (fluvial-dominated delta) (Figure 9). The siliciclastic platform was in regression during the Middle Triassic. The Lower Landa Member of the Tredian Formation shows deposition of sandstone

in distributary channels or inter-distributary bays with associated shales in a low-energy setting, such as a floodplain or marshes (Figure 9). It is followed by the deposition of thick channelized sandstone in the Khatkiara Member with a dominant fluvial character. The thick sandstone of the Khatkiara Member is the result of high-density channel flow showing a fining upward sequence. This period is marked by maximum regression, during which the depositional environment changed from deltaic to fluvio-deltaic. Directional features, i.e., cross-beds, indicate channel flow from the southeast. The presence of carbonaceous clays indicates deposition in an overbank area (swamps and marshes). The top of the channelized sandstone shows a transition from thick channelized deposits to thin tide-dominated deposits, i.e., rhythmites (Figure 9). The top of the Khatkiara Member contains a few dolomite beds indicating tidal environments, followed up by the thick dolomite deposits of the Kingriali Formation. This shows that the deposition of Mid-Triassic rocks took place at a time marked by a fall in regional base level and more clastic input. Finally, during the Late Triassic, a major rise in the regional base level terminated the siliciclastic system and started depositing carbonates in the overlying Kingriali Formation.

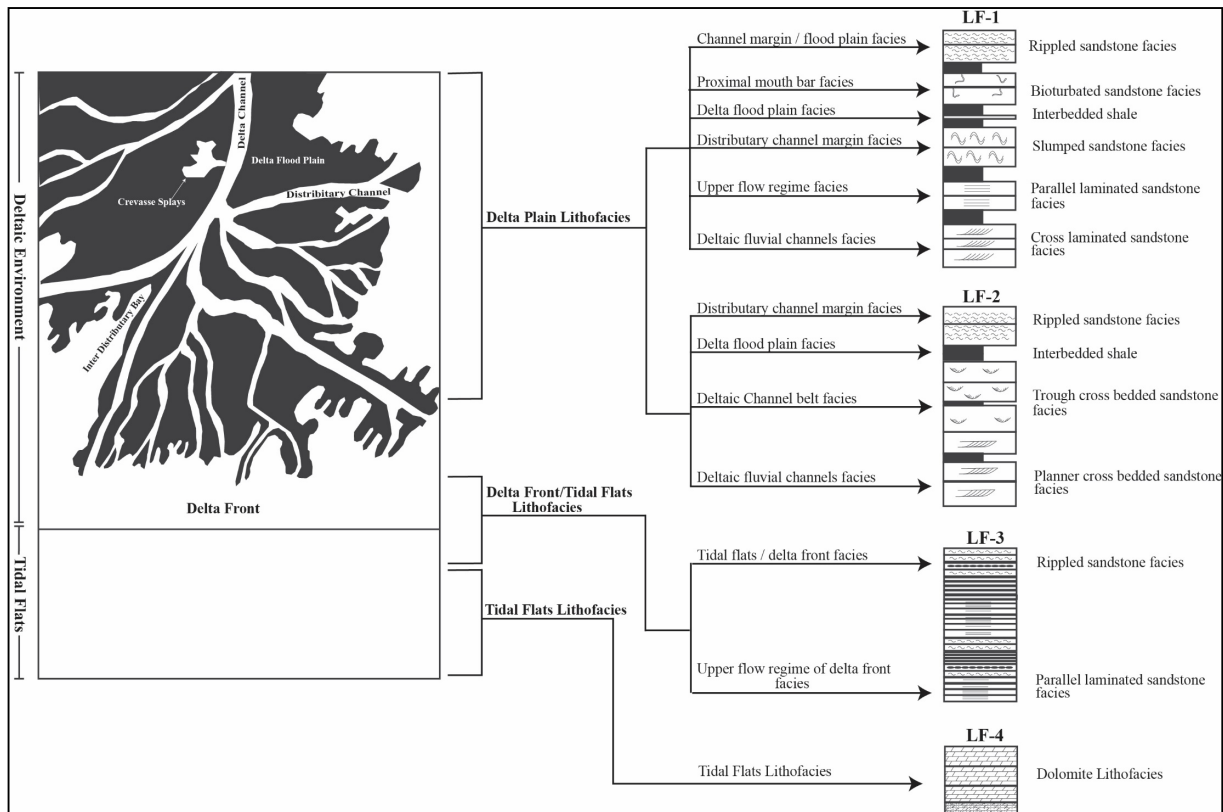


**Figure 9.** Depositional model of Tredian Formation indicative of a fluvio-deltaic environment showing the regional location with its dominant characteristics such as facies association, composition, and distribution of the studied sandstones.

### 5.3. Paragenetic Sequence

The paragenetic sequence of the Tredian Formation was determined based on petrographic and SEM observations. The paragenetic sequence inferred for the Tredian sandstone is shown in Figure 10. The Tredian sandstone has survived intense and complex diagenetic phases (early, late, and uplift). The earliest diagnostic events occurred soon after deposition, and the latest ones are those occurring currently.

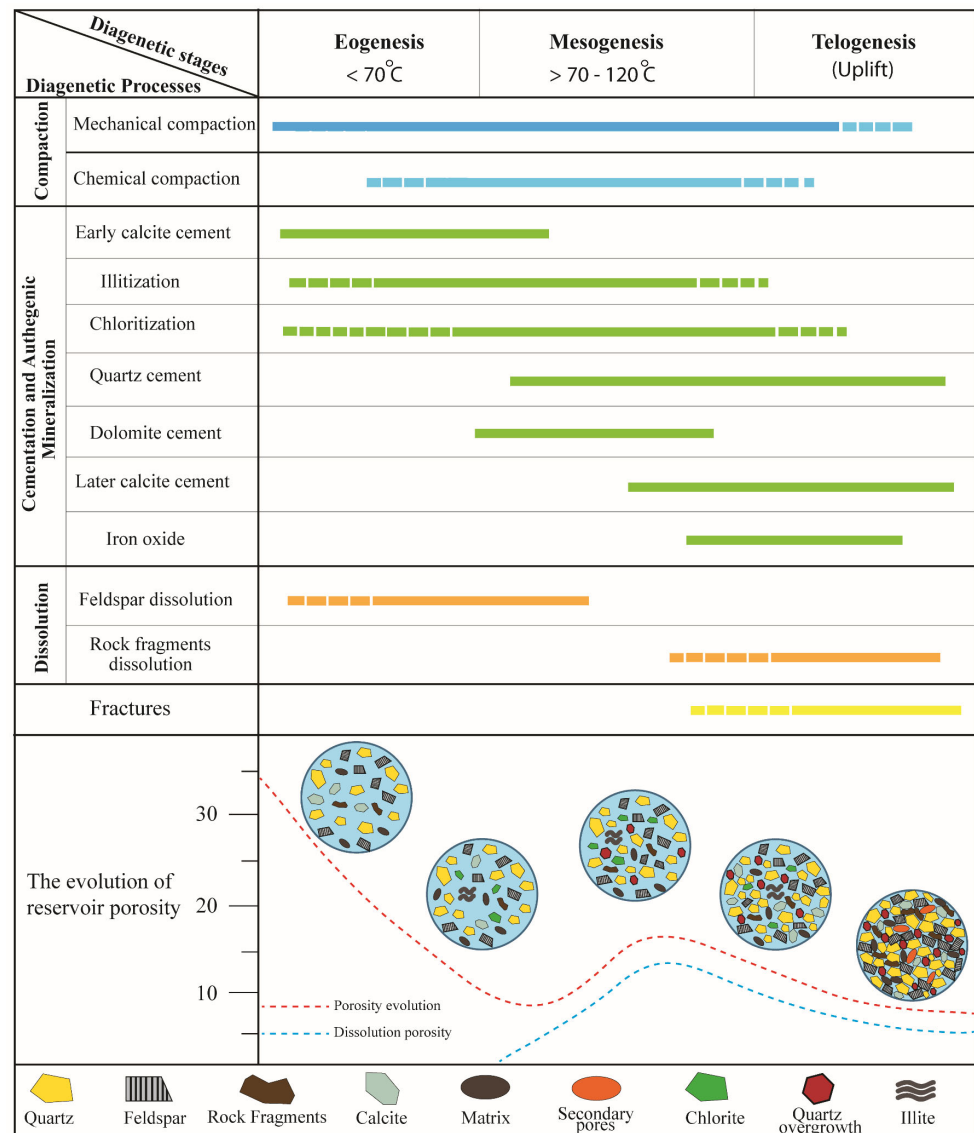


**Figure 10.** Diagenetic model showing the relationship of various diagenetic stages and evolution of porosity with time [73].

The sequence of inferred major diagenetic processes distinguished in the studied sandstone is as follows:

Early mechanical compaction is the first diagnostic event, which is evident from the tight grain packing of sandstone [74] (Figure 7b,f). Mechanical compaction typically occurs from the early-to-late diagenetic stages [75]. However, the early precipitation of massive poikilotopic calcite cement in the Landa Member prevented further compaction (Figure 8a). The rarity of calcite cement made possible the continuation of compaction through later diagenetic stages in the Khatkiara Member. Mechanical compaction is also evident from the breaking down of grains (Figure 7m). After compaction and calcite cementation, dissolution of unstable grains, such as feldspars or alteration of feldspar to clays, possibly due to the influx of meteoric water, is an important event (Figure 8o) [76,77].

Illitization and chloritization constitute the next diagenetic stage and are time- and temperature-dependent [34]. Illite may have been formed by decomposing the feldspar grains or by clay mineral transformation, i.e., smectite and kaolinite illitization. The absence of quartz overgrowth from samples containing chlorite as grain coating indicates the latter to be an earlier diagenetic product (Figure 8g). The relationship between illite and chlorite is not clear. The occurrence of chlorite on quartz grains without overgrowth shows chlorite

obstruction in the formation of overgrowth. Quartz overgrowth is late-stage diagenetic cement and usually precipitates on clean surfaces (Figure 8c). The quartz overgrowth is impeded by the precipitation of dolomite. The possible sources of silica may include pressure solution, dissolution of framework grains, feldspar replacement, or transported silica-rich fluids. In addition to the early calcite cementation, another generation of pore-filling calcite cement (formed during burial diagenesis) took place after the quartz and dolomite cementation and led to corrosion of the dolomite cement. Following the precipitation of iron oxide or hydroxide and the dissolution of grains and cements, grain fracturing was the most recent diagenetic event. Grain fracturing postdates late-stage calcite cement as the fractures are not filled and may be related to uplifting (Figure 8o). During the process of uplifting (telogenesis) [6], ferruginous cement precipitated and engulfed other diagenetic products, especially calcite and dolomite cements. The patchy appearance and uneven distribution of iron-oxide cements indicate surface weathering-related infiltration during the telogenetic stage [78]. The secondary porosity has been created in the studied sandstone due to the dissolution of grains as well as authigenic cements.

#### 5.4. Reservoir Characterization

Reservoir characterization of sandstone refers to the amount of porosity and permeability it retained after diagenetic processes and is a function of depositional and diagenetic control [79,80]. Burial diagenesis most likely affects the reservoir quality of sandstone. The diagenetic processes, which may either reduce porosity and permeability by physical compaction and authigenic cementation or enhance porosity by the unstable grains and cement dissolution, largely determine the reservoir quality of sandstone [81–83]. The real benefit of secondary porosity for reservoirs is rare as the dissolved material may precipitate as cement in the sandstone [84]. Thin sections stained with blue epoxy were used to estimate the visual porosity of sandstone by point counting along with some SEM images. Although the porosity of examined samples of sandstone is highly affected by compaction, cementation, and authigenic clay mineral formation, it is dominated by inter- and intra-granular pores, dissolution, and fractured pores (secondary porosity). The estimated visual point-count porosity values for the sandstone vary between 0.5 and 16%, averaging 6%. The processes of mechanical compaction and early calcite cementation in the Landa Member have appreciably reduced the primary porosity of the Tredian sandstone (Figure 8a). Due to the rarity of calcite cement, the Khatkiara Member of the Tredian sandstone continued to experience mechanical compaction to greater depths and thus attained closer grain packing (long to concavo-convex) (Figure 8b). The initial porosity reduction was due to mechanical compaction that continued to take place in the samples containing little calcite cement. The inter-granular volume (IGV) of sandstone is decreased by the processes of physical and chemical compaction, as evidenced by the tight grain packing.

The role of chlorite precipitation, either in pore spaces or on grain surfaces, may also contribute to either the reduction or preservation of porosity in the sandstone of the Tredian Formation. The porosity is preserved in the sandstone samples, where quartz overgrowth was prevented due to precipitation of chlorite on grain surfaces (Figure 8g). Chlorite precipitation in the pore spaces reduces permeability, but the rosette form of chlorite possesses inter-crystalline porosity (Figure 11).

The fibrous illite blocks the pore spaces and thus reduces the reservoir properties. Fractures produced due to physical compaction also opened due to dissolution and contributed significantly to the overall porosity of the sandstone [85]. An excessive number of unstable grains have undergone dissolution during the diagenesis of sandstone (Figure 11c). Dissolution of feldspar grains, volcanic fragments, and cements created secondary porosity during the early-to-late stages of diagenesis (Figure 11d). It is observed that the authigenic (calcite) cements partly to completely fill the secondary pores produced as a result of grain dissolution during early diagenesis. Additionally, the late-stage grain and cement dissolution has created and preserved good visual secondary porosity, as observed in the thin sections, and further confirmed through SEM images (Figure 11a–f).

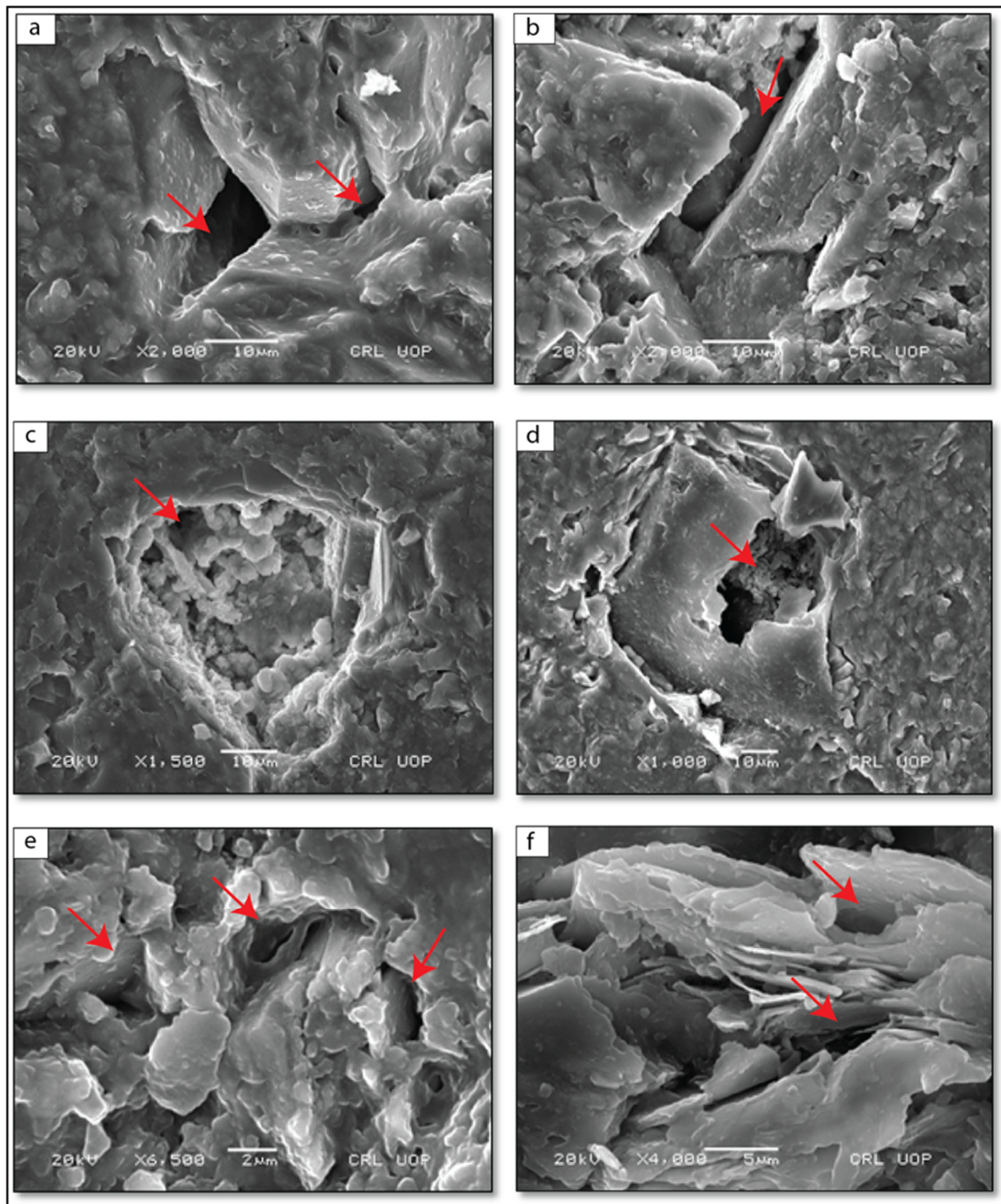


**Figure 11.** SEM images showing different types of porosity (Red arrow). (a) SEM image showing inter-granular porosity between the framework grains in tight packing (arrow indicate porosity). (b) SEM image showing porosity between the framework grains. (c) SEM image showing dissolution porosity filled with chlorite. (d) SEM image showing secondary porosity generated as a result of partial dissolution of carbonate grain. (e) SEM image showing secondary porosity between the framework grains (Red arrow). (f) SEM image showing inter-crystalline porosity between the rosette chlorite (Red arrow).

According to Khan et al. [86], the distribution of attributes such as the thickness of the sandstone body and its sand percentage along with the internal architecture, heterogeneity, sand body geometries, and their constituent facies may also influence the reservoir characteristics. Thicker sandstone strata usually show high porosity values; however, prevailing depositional environments and sediment influx determine the sand body thickness. Table 3 shows the reservoir quality of the Tredian Formation lithofacies.

**Table 3.** Reservoir quality characteristics of different lithofacies of Tredian Formation.

Lithofacies	Type of Porosity	Degree of Compaction	Cementing Material and Authigenic Clays	Reservoir Quality
Lithofacies 1 (LF-1)	No visual porosity because all the intergranular pores are filled with cement	Moderate to tight compaction of grains	Poikilotopic cement is filled in pore spaces, quartz overgrowth is not seen	Poor reservoir
Lithofacies 2 (LF-2)	Intergranular and dissolution porosity	Moderately packed grains	Pores are filled with late-stage ferruginous cement. Chlorite is seen as grain coating. Illite is also present in pore spaces	Good reservoir
Lithofacies 3 (LF-3)	Secondary fracture and dissolution porosity is observed	Loose–moderate packing of grains	Well-developed quartz overgrowth. Clay rims around few grains	Good reservoir
Lithofacies 4 (LF-4)	Fractures or any other dissolution cavities are not observed	Highly compacted	Calcite and dolomite cement is observed	Poor reservoir

### 6. Conclusions

The studied Tredian Formation has been sub-divided into sandstone interbedded with shale lithofacies (LF1), thick-bedded sandstone lithofacies (LF2), thin-bedded sandstone lithofacies (LF3), and dolomite lithofacies (LF4). The distinguished facies associations were interpreted as fluvio-deltaic and tidal flat settings. The characteristic four lithofacies show deposition in delta plain, fluvial channels, and tidal flat environments. The Tredian Formation in the Salt and Trans-Indus Surghar Ranges was the result of overall regression (progradation) during the Mid-Triassic. The falling sea level has supplied the required abundant sandy input. The environment of deposition for the study of Tredian Formation is a fluvial dominated delta. The characteristics depositional processes are both fluvial and marine. The sandstone of the Tredian Formation has been classified as sub-feldspathic arenite to feldspathic arenite based on petrography. Petrographic observations show that the Tredian sandstone has experienced all phases of diagenesis, i.e., shallow to deep burial followed by uplifting. These diagenetic changes have affected the reservoir properties of the Tredian Formation. The major diagenetic signatures observed in the Tredian sandstone are chemical and mechanical compaction, authigenic mineralization, cementation (calcite, silica, dolomite, and ferruginous), replacement, grain fracturing and dissolution. Early cementation has destroyed all the visible porosity in the lithofacies LF1 by enclosing all the grains. This lithofacies entirely consist of the Landa Member. No further clues of later dissolution were observed in samples from this lithofacies. Lithofacies LF2 and LF3, part of the Khatkiara Member, display good visible porosity, which is also confirmed by SEM analysis. The presence of a chlorite rim around some grains served to preserve porosity by inhibiting quartz overgrowth; however, quartz cementation and overgrowth are present in some samples. Moreover, the processes of dissolution and grain fracturing (later in diagenesis) have created enough secondary porosity and made the sandstone a suitable hydrocarbon reservoir. Lithofacies LF4 is dolomitic facies containing some floating framework grains but it shows no visible porosity and suggests the start of marine conditions after regression. Finally, ferruginous cementation during the last stage of diagenesis has destroyed the reservoir properties of the Tredian sandstone in specific zones; however, dissolution of framework grains, fractures, and cements (calcite, silica, dolomite, and ferruginous) have created secondary porosity.

**Author Contributions:** Conceptualization, K.A.Q. and M.A.; methodology, K.A.Q., M.A. and A.B.; software, K.A.Q., M.A., H.T.J. and G.K.; validation, K.A.Q., M.A., H.T.J., G.K. and S.A.; formal

analysis, K.A.Q., M.A. and S.A.; investigation, K.A.Q., M.A. and G.K.; resources, M.A. and S.A.; data curation, K.A.Q., M.A. and G.K.; writing—original draft preparation, K.A.Q. and M.A.; writing—review and editing, H.T.J. and G.K.; visualization, M.A.; supervision, M.A.; project administration, M.A.; funding acquisition, H.T.J. and G.K. All authors have read and agreed to the published version of the manuscript.

**Funding:** This research was funded by the Higher Education Commission (HEC) of Pakistan under Access to Scientific Instrumentation Programme (ASIP) (HEC Award Letter No: 20-2(3)/HDIP, Ibd/ASIP/R&D/HEC/2016/630).

**Institutional Review Board Statement:** Not applicable.

**Informed Consent Statement:** Not applicable.

**Data Availability Statement:** The authors confirm that the data supporting the findings of this study are available within the article.

**Acknowledgments:** K.A.Q. is extremely thankful to Nowrad Ali (University of Peshawar) for his help during fieldwork. We are thankful to the Department of Earth Sciences, COMSATS Abbottabad for providing access to Lab instrumentation.

**Conflicts of Interest:** The authors declare no conflict of interest.

## References

- Miall, A.D. Stratigraphic sequences and their chronostratigraphic correlation. *J. Sediment. Res.* **1991**, *61*, 497–505.
- Bjørlykke, K. Relationships between depositional environments, burial history, and rock properties. Some principal aspects of diagenetic process in sedimentary basins. *Sediment. Geol.* **2014**, *301*, 1–14. [[CrossRef](#)]
- Dickinson, W.R. Interpreting provenance relations from detrital modes of sandstones. In *Provenance of Arenites*; D. Reidel Publishing Company: Dordrecht, The Netherlands, 1985; pp. 333–361.
- Dixon, S.A.; Summers, D.M.; Surdam, R.C. Diagenesis and preservation of porosity in Norphlet Formation (Upper Jurassic), southern Alabama. *AAPG Bull.* **1989**, *73*, 707–728.
- Taylor, T.R.; Giles, M.R.; Hathon, L.A.; Diggs, T.N.; Braunsdorf, N.R.; Birbiglia, G.V.; Kittridge, M.G.; Macaulay, C.I.; Espejo, I.S. Sandstone diagenesis and reservoir quality prediction: Models, myths, and reality. *AAPG Bull.* **2010**, *94*, 1093–1132. [[CrossRef](#)]
- Khan, S.D.; Chen, L.; Ahmad, S.; Ahmad, I.; Ali, F. Lateral structural variation along the Kalabagh Fault Zone, NW Himalayan foreland fold-and-thrust belt, Pakistan. *J. Asian Earth Sci.* **2012**, *50*, 79–87. [[CrossRef](#)]
- Shah, S. *Stratigraphy of Pakistan (Memoirs of the Geological Survey of Pakistan)*; Geological Survey of Pakistan: Quetta, Pakistan, 2009; Volume 22.
- Bilal, A.; Yang, R.; Janjuhah, H.T.; Mughal, M.S.; Li, Y.; Kontakiotis, G.; Lenhardt, N. Microfacies analysis of the Palaeocene Lockhart limestone on the eastern margin of the Upper Indus Basin (Pakistan): Implications for the depositional environment and reservoir characteristics. *Depos. Rec.* **2023**, *9*, 152–173. [[CrossRef](#)]
- Bilal, A.; Mughal, M.S.; Janjuhah, H.T.; Ali, J.; Niaz, A.; Kontakiotis, G.; Antonarakou, A.; Usman, M.; Hussain, S.A.; Yang, R. Petrography and Provenance of the Sub-Himalayan Kuldana Formation: Implications for Tectonic Setting and Palaeoclimatic Conditions. *Minerals* **2022**, *12*, 794. [[CrossRef](#)]
- Qureshi, K.A.; Hussain, H.; Shah, A.A.; Meerani, I.A.; Fahad, S.; Basit, A. Hydrocarbon Source and Reservoir Rock Potential of the Paleocene Hangu Formation in the Himalayan Foreland Basin, North West Pakistan: Insight from Geochemical and Diagenetic Study: Geochemical and Diagenetic Study of Hangu Formation. *Pak. J. Sci. Ind. Res. Ser. A Phys. Sci.* **2019**, *62*, 157–166. [[CrossRef](#)]
- Ishaq, K.; Wahid, S.; Yaseen, M.; Hanif, M.; Ali, S.; Ahmad, J.; Mehmood, M. Analysis of subsurface structural trend and stratigraphic architecture using 2D seismic data: A case study from Bannu Basin, Pakistan. *J. Pet. Explor. Prod.* **2021**, *11*, 1019–1036. [[CrossRef](#)]
- Khan, M.Z.; Khan, M.R.; Raza, A. Reservoir Potential of Marwat and Khisor Trans Indus Ranges, Northwest Pakistan. In Proceedings of the AAPG International Conference & Exhibition, Istanbul, Turkey, 14–17 September 2014.
- Shahtakhtinskiy, A.; Khan, S. Quantitative analysis of facies variation using ground-based lidar and hyperspectral imaging in Mississippian limestone outcrop near Jane, Missouri. *Interpretation* **2020**, *8*, T365–T378. [[CrossRef](#)]
- Shahtakhtinskiy, A.; Khan, S. 3D stratigraphic mapping and reservoir architecture of the Balakhany Suite, Upper Productive Series, using UAV photogrammetry: Yasamal Valley, Azerbaijan. *Mar. Pet. Geol.* **2022**, *145*, 105911. [[CrossRef](#)]
- Morad, S.; Al-Ramadan, K.; Ketzner, J.M.; De Ros, L. The impact of diagenesis on the heterogeneity of sandstone reservoirs: A review of the role of depositional facies and sequence stratigraphy. *AAPG Bull.* **2010**, *94*, 1267–1309. [[CrossRef](#)]
- Salah, M.K.; Janjuhah, H.; Sanjuan, J.; Maalouf, E. Impact of diagenesis and pore aspects on the petrophysical and elastic properties of carbonate rocks from southern Lebanon. *Bull. Eng. Geol. Environ.* **2023**, *82*, 67. [[CrossRef](#)]
- Sitholey, R. Plant remains from the Triassic of the Salt Range, Punjab. *Proc. Nat. Acad. Sci. India* **1943**, *13*, 300–327.
- Sarjeant, W. Acritarchs and Tasmanitids from the Mianwali and Tredian Formations (Triassic) of the Salt and Surghar Ranges, West Pakistan. 1973. Available online: <https://eurekamag.com/research/037/751/037751535.php> (accessed on 1 May 2023).

19. Hermann, E.; Hochuli, P.A.; Bucher, H.; Roohi, G. Uppermost Permian to Middle Triassic palynology of the Salt Range and Surghar Range, Pakistan. *Rev. Palaeobot. Palynol.* **2012**, *169*, 61–95. [[CrossRef](#)]
20. Khan, S.; Ahmad, W.; Ahmad, S.; Khan, J.K. Dating and depositional environment of the Tredian Formation, western Salt Range, Pakistan. *J. Himal. Earth Sci.* **2016**, *49*, 14–25.
21. Treloar, P.J.; Izatt, C.N. Tectonics of the Himalayan collision between the Indian plate and the Afghan block: A synthesis. *Geol. Soc. Lond. Spec. Publ.* **1993**, *74*, 69–87. [[CrossRef](#)]
22. Yin, A. Cenozoic tectonic evolution of the Himalayan orogen as constrained by along-strike variation of structural geometry, exhumation history, and foreland sedimentation. *Earth-Sci. Rev.* **2006**, *76*, 1–131. [[CrossRef](#)]
23. Ali, S.K.; Lashari, R.A.; Sahito, A.G.; Kontakiotis, G.; Janjuhah, H.T.; Mughal, M.S.; Bilal, A.; Mehmood, T.; Majeed, K.U. Sedimentological and Petrographical Characterization of the Cambrian Abbottabad Formation in Kamsar Section, Muzaffarabad Area: Implications for Proto-Tethys Ocean Evolution. *J. Mar. Sci. Eng.* **2023**, *11*, 526. [[CrossRef](#)]
24. Islam, F.; Ahmad, M.N.; Janjuhah, H.T.; Ullah, M.; Islam, I.U.; Kontakiotis, G.; Skilodimou, H.D.; Bathrellos, G.D. Modelling and Mapping of Soil Erosion Susceptibility of Murree, Sub-Himalayas Using GIS and RS-Based Models. *Appl. Sci.* **2022**, *12*, 12211. [[CrossRef](#)]
25. Kazmi, A.; Qasimjan, M. *Geology and Tectonics of Pakistan*; SI Graphic Publishes: Karachi, Pakistan, 1997.
26. Jaumé, S.C.; Lillie, R.J. Mechanics of the Salt Range-Potwar Plateau, Pakistan: A fold-and-thrust belt underlain by evaporites. *Tectonics* **1988**, *7*, 57–71. [[CrossRef](#)]
27. McDougall, J.W.; Khan, S.H. Strike-slip faulting in a foreland fold-thrust belt: The Kalabagh Fault and Western Salt Range, Pakistan. *Tectonics* **1990**, *9*, 1061–1075. [[CrossRef](#)]
28. Bilal, A.; Yang, R.; Mughal, M.S.; Janjuhah, H.T.; Zaheer, M.; Kontakiotis, G. Sedimentology and Diagenesis of the Early–Middle Eocene Carbonate Deposits of the Ceno-Tethys Ocean. *J. Mar. Sci. Eng.* **2022**, *10*, 1794. [[CrossRef](#)]
29. Zaheer, M.; Khan, M.R.; Mughal, M.S.; Janjuhah, H.T.; Makri, P.; Kontakiotis, G. Petrography and Lithofacies of the Siwalik Group in the Core of Hazara-Kashmir Syntaxis: Implications for Middle Stage Himalayan Orogeny and Paleoclimatic Conditions. *Minerals* **2022**, *12*, 1055. [[CrossRef](#)]
30. Gee, E.; Gee, D. Overview of the geology and structure of the Salt Range, with observations on related areas of northern Pakistan. *Geol. Soc. Am. Spec. Pap.* **1989**, *232*, 95–112.
31. Ahmad, S.; Ali, A.; Khan, M.I. Imprints of transtensional deformation along Kalabagh fault in the vicinity of Kalabagh Hills, Pakistan. *Pak. J. Hydrocarb. Res.* **2005**, *15*, 35–42.
32. Powell, C.M. *A Speculative Tectonic History of Pakistan and Surroundings*; Geodynamics of Pakistan: Quetta, Pakistan, 1979; pp. 5–24.
33. Ahmad, I.; Shah, M.M.; Janjuhah, H.T.; Trave, A.; Antonarakou, A.; Kontakiotis, G. Multiphase Diagenetic Processes and Their Impact on Reservoir Character of the Late Triassic (Rhaetian) Kingriali Formation, Upper Indus Basin, Pakistan. *Minerals* **2022**, *12*, 1049. [[CrossRef](#)]
34. Humphreys, B.; Smith, S.; Strong, G. Authigenic chlorite in late Triassic sandstones from the Central Graben, North Sea. *Clay Miner.* **1989**, *24*, 427–444. [[CrossRef](#)]
35. Golonka, J.; Ford, D. Pangean (late Carboniferous–Middle Jurassic) paleoenvironment and lithofacies. *Palaeogeogr. Palaeoclimatol. Palaeoecol.* **2000**, *161*, 1–34. [[CrossRef](#)]
36. Basit, A.; Umar, M.; Jamil, M.; Qasim, M. Facies analysis and depositional framework of Late Permian–Jurassic sedimentary successions, Western Salt Range, Pakistan: Implications for sequence stratigraphic trends and paleogeography of the Neo-Tethys Sea. *Kuwait J. Sci.* **2023**, *50*, 1–12. [[CrossRef](#)]
37. Ali, S.K.; Janjuhah, H.T.; Shahzad, S.M.; Kontakiotis, G.; Saleem, M.H.; Khan, U.; Zarkogiannis, S.D.; Makri, P.; Antonarakou, A. Depositional Sedimentary Facies, Stratigraphic Control, Paleocological Constraints, and Paleogeographic Reconstruction of Late Permian Chhidru Formation (Western Salt Range, Pakistan). *J. Mar. Sci. Eng.* **2021**, *9*, 1372. [[CrossRef](#)]
38. Balme, B.E. *Palynology of Permian and Triassic Strata in the Salt Range and Surghar Range, West Pakistan*; University Press of Kansas: Lawrence, KS, USA, 1970; Volume 4.
39. Janjuhah, H.T.; Alansari, A.; Santha, P.R. Interrelationship between facies association, diagenetic alteration and reservoir properties evolution in the Middle Miocene carbonate build up, Central Luconia, Offshore Sarawak, Malaysia. *Arab. J. Sci. Eng.* **2019**, *44*, 341–356. [[CrossRef](#)]
40. Garzanti, E.; Vezzoli, G.; Andò, S.; Paparella, P.; Clift, P.D. Petrology of Indus River sands: A key to interpret erosion history of the Western Himalayan Syntaxis. *Earth Planet. Sci. Lett.* **2005**, *229*, 287–302. [[CrossRef](#)]
41. Pettijohn, F. *Sedimentary Rocks*, 3rd ed.; Herper & Row: New York, NY, USA, 1975; Volume 614.
42. Morad, S. Carbonate cementation in sandstones: Distribution patterns and geochemical evolution. In *Carbonate Cementation in Sandstones: Distribution Patterns and Geochemical Evolution*; Wiley Publisher: Hoboken, NJ, USA, 1998; pp. 1–26.
43. Burton, J.; Krinsley, D.; Pye, K. Authigenesis of kaolinite and chlorite in Texas Gulf Coast sediments. *Clays Clay Miner.* **1987**, *35*, 291–296. [[CrossRef](#)]
44. Hayes, J.B. Polytypism of chlorite in sedimentary rocks. *Clays Clay Miner.* **1970**, *18*, 285–306. [[CrossRef](#)]
45. Warren, E.; Curtis, C. The chemical composition of authigenic illite within two sandstone reservoirs as analysed by ATEM. *Clay Miner.* **1989**, *24*, 137–156. [[CrossRef](#)]

46. Coleman, J.M.; Gagliano, S.M. Cyclic Sedimentation in the Mississippi River Deltaic Plain. 1964. Available online: <https://www.semanticscholar.org/paper/Cyclic-sedimentation-in-the-Mississippi-River-Gulf-Coleman-Gagliano/ce137f9553108982f02f6680db1e11c40a47c19c> (accessed on 1 May 2023).
47. Olariu, C.; Bhattacharya, J.P. Terminal distributary channels and delta front architecture of river-dominated delta systems. *J. Sediment. Res.* **2006**, *76*, 212–233. [[CrossRef](#)]
48. Kästner, K.; Hoitink, A.; Vermeulen, B.; Geertsema, T.; Ningsih, N. Distributary channels in the fluvial to tidal transition zone. *J. Geophys. Res. Earth Surf.* **2017**, *122*, 696–710. [[CrossRef](#)]
49. Reading, H.; Levell, B. Controls on the sedimentary rock record. *Sediment. Environ. Process. Facies Stratigr.* **1996**, *3*, 5–36.
50. Oomkens, E. *Depositional Sequences and Sand Distribution in the Postglacial Rhone Delta Complex*; SEPM Sociert of Sedmentart Geology: Broken Arrow, OK, USA, 1970; Volume 15.
51. Oomkens, E. Lithofacies relations in the Late Quaternary Niger delta complex. *Sedimentology* **1974**, *21*, 195–222. [[CrossRef](#)]
52. Coleman, J. *Deltas: Processes and Models of Deposition for Exploration*; Burgess CEPCO Division: Minneapolis, MN, USA; Springer: Heidelberg, The Neatherlands, 1981; Volume 124.
53. Swift, D.J.; Figueiredo, A.G.; Freeland, G.; Oertel, G. Hummocky cross-stratification and megaripples; a geological double standard? *J. Sediment. Res.* **1983**, *53*, 1295–1317.
54. Boggs, S., Jr.; Boggs, S. *Petrology of Sedimentary Rocks*; Cambridge University Press: Cambridge, UK, 2009.
55. Eriksson, P.G.; Condie, K.C.; Tirsgaard, H.; Mueller, W.; Altermann, W.; Miall, A.D.; Aspler, L.B.; Catuneanu, O.; Chiarenzelli, J.R. Precambrian clastic sedimentation systems. *Sediment. Geol.* **1998**, *120*, 5–53. [[CrossRef](#)]
56. Nichols, G. SELLEY, RC 2000. Applied Sedimentology, x+ 523 pp. San Diego, San Francisco, New York, Boston, London, Sydney, Tokyo: Academic Press. Price US \$82.50 (hard covers). ISBN 0 12 636375 7. *Geol. Mag.* **2001**, *138*, 619–630. [[CrossRef](#)]
57. Mehmood, M.; Naseem, A.A.; Saleem, M.; Rehman, J.; Kontakiotis, G.; Janjuhah, H.T.; Khan, E.; Antonarakou, A.; Khan, I.; Rehman, A.; et al. Sedimentary Facies, Architectural Elements and Depositional Environments of the Maastrichtian Pab Formation in the Rakhi Gorge, Eastern Sulaiman Ranges, Pakistan. *J. Mar. Sci. Eng.* **2023**, *11*, 726. [[CrossRef](#)]
58. Allison, M.A.; Khan, S.; Goodbred, S.L., Jr.; Kuehl, S.A. Stratigraphic evolution of the late Holocene Ganges–Brahmaputra lower delta plain. *Sediment. Geol.* **2003**, *155*, 317–342. [[CrossRef](#)]
59. Scasso, R.; Aberhan, M.; Ruiz, L.; Weidemeyer, S.; Medina, F.; Kiessling, W. Integrated bio-and lithofacies analysis of coarse-grained, tide-dominated deltaic environments across the Cretaceous/Paleogene boundary in Patagonia, Argentina. *Cretac. Res.* **2012**, *36*, 37–57. [[CrossRef](#)]
60. Aitken, J.F.; Flint, S.S. *High-Frequency Sequences and the Nature of Incised-Valley Fills in Fluvial Systems of the Breathitt Group (Pennsylvanian), Appalachian Foreland Basin, Eastern Kentucky*; Special Publication No. 51; Society of Economic Paleontologists and Mineralogists: Tulsa, OK, USA, 1994; pp. 353–368.
61. Reineck, H.; Singh, I. Der Golf von Gaeta (Tyrrhenisches Meer); III, Die Gefuege von Vorstrand-und Schelfsedimenten. *Senckenberg. Marit.* **1971**, *3*, 185–194.
62. Wunderlich, F. Georgia Coastal Region, Sapelo Island, USA: Sedimentology and Biology. III. Beach Dynamics and Beach Development. 1972. Available online: <https://pascal-francis.inist.fr/vibad/index.php?action=getRecordDetail&idt=PASCALGEODEBRGM732262573> (accessed on 1 May 2023).
63. Desjardins, P.R.; Buatois, L.A.; Limarino, C.O.; Cisterna, G.A. Latest Carboniferous–earliest Permian transgressive deposits in the Paganzo Basin of western Argentina: Lithofacies and sequence stratigraphy of a coastal-plain to bay succession. *J. S. Am. Earth Sci.* **2009**, *28*, 40–53. [[CrossRef](#)]
64. Boggs, S., Jr. *Principal of Sedimentology and Stratigraphy 4th Edition, Hal 550–553*; Pearson Prentice Hall: Upper Saddle River, NJ, USA, 2006.
65. Reineck, H.E.; Wunderlich, F. Classification and origin of flaser and lenticular bedding. *Sedimentology* **1968**, *11*, 99–104. [[CrossRef](#)]
66. Reineck, H.-E.; Singh, I.B. *Depositional Sedimentary Environments: With Reference to Terrigenous Clastics*; Springer Science & Business Media: Berlin/Heidelberg, Germany, 2012.
67. Terwindt, J. *Lithofacies of Inshore Estuarine and Tidal Inlet Deposits: Geologie & Mijnbouw*; Publicatie uit het Geografisch Instituut der Rijksuniversiteit te Utrecht: Utrecht, The Netherlands, 1971; Volume 50.
68. Hermann, E.; Hochuli, P.A.; Bucher, H.; Vigran, J.O.; Weissert, H.; Bernasconi, S.M. A close-up view of the Permian–Triassic boundary based on expanded organic carbon isotope records from Norway (Trøndelag and Finnmark Platform). *Glob. Planet. Chang.* **2010**, *74*, 156–167. [[CrossRef](#)]
69. Rahim, H.-U.; Qamar, S.; Shah, M.M.; Corbella, M.; Martín-Martín, J.D.; Janjuhah, H.T.; Navarro-Ciurana, D.; Lianou, V.; Kontakiotis, G. Processes Associated with Multiphase Dolomitization and Other Related Diagenetic Events in the Jurassic Samana Suk Formation, Himalayan Foreland Basin, NW Pakistan. *Minerals* **2022**, *12*, 1320. [[CrossRef](#)]
70. Lagaaij, R.; Kopstein, F. Typical features of a fluvio-marine offlap sequence. In *Developments in Sedimentology*; Elsevier: Amsterdam, The Netherlands, 1964; Volume 1, pp. 216–226.
71. Penland, S.; Boyd, R.; Suter, J.R. Transgressive depositional systems of the Mississippi Delta plain; a model for barrier shoreline and shelf sand development. *J. Sediment. Res.* **1988**, *58*, 932–949.
72. Carrión-Torrente, Á.; Lobo, F.J.; Puga-Bernabéu, Á.; Mendes, I.; Lebreiro, S.; García, M.; van Rooij, D.; Luján, M.; Reguera, M.I.; Antón, L. Episodic postglacial deltaic pulses in the Gulf of Cadiz: Implications for the development of a transgressive shelf and driving environmental conditions. *J. Sediment. Res.* **2022**, *92*, 1116–1140. [[CrossRef](#)]

73. Dowe, P.J.; Taylor, K.G. Diagenetic mineral development within the Upper Jurassic Haynesville-Bossier Shale, USA. *Sedimentology* **2020**, *67*, 47–77. [[CrossRef](#)]
74. Barshep, D.V.; Worden, R.H. Reservoir Quality of Upper Jurassic Corallian Sandstones, Weald Basin, UK. *Geosciences* **2021**, *11*, 446. [[CrossRef](#)]
75. Salah, M.K.; Janjuhah, H.T.; Sanjuan, J. Analysis and Characterization of Pore System and Grain Sizes of Carbonate Rocks from Southern Lebanon. *J. Earth Sci.* **2023**, *34*, 101–121. [[CrossRef](#)]
76. Wang, Y.; Cheng, H.; Hu, Q.; Liu, L.; Hao, L. Diagenesis and pore evolution for various lithofacies of the Wufeng-Longmaxi shale, southern Sichuan Basin, China. *Mar. Pet. Geol.* **2021**, *133*, 105251. [[CrossRef](#)]
77. Fathy, D.; El-Balkiemy, A.F.; Makled, W.A.; Hosny, A.M. Organic geochemical signals of Paleozoic rocks in the southern Tethys, Siwa basin, Egypt: Implications for source rock characterization and petroleum system. *Phys. Chem. Earth Parts A/B/C* **2023**, *130*, 103393. [[CrossRef](#)]
78. Fathy, D.; Abart, R.; Wagreeich, M.; Gier, S.; Ahmed, M.S.; Sami, M. Late campanian climatic-continental weathering assessment and its influence on source rocks deposition in southern Tethys, Egypt. *Minerals* **2023**, *13*, 160. [[CrossRef](#)]
79. Yang, Y. Reservoir characteristics and controlling factors of the Lower paleogene sandstones in the southeast part of Jiyang Sag, BohaiBay Basin, China. *Alex. Eng. J.* **2022**, *61*, 10277–10282. [[CrossRef](#)]
80. Jafarzadeh, N.; Kadkhodaie, A.; Bahrehvar, M.; Wood, D.A.; Janahmad, B. Reservoir characterization of fluvio-deltaic sandstone packages in the framework of depositional environment and diagenesis, the south Caspian Sea basin. *J. Asian Earth Sci.* **2022**, *224*, 105028. [[CrossRef](#)]
81. Chen, J.; Yao, J.; Mao, Z.; Li, Q.; Luo, A.; Deng, X.; Shao, X. Sedimentary and diagenetic controls on reservoir quality of low-porosity and low-permeability sandstone reservoirs in Chang101, upper Triassic Yanchang Formation in the Shanbei area, Ordos Basin, China. *Mar. Pet. Geol.* **2019**, *105*, 204–221. [[CrossRef](#)]
82. Burley, S.; Kantorowicz, J. Thin section and SEM textural criteria for the recognition of cement-dissolution porosity in sandstones. *Sedimentology* **1986**, *33*, 587–604. [[CrossRef](#)]
83. Janjuhah, H.T.; Kontakiotis, G.; Wahid, A.; Khan, D.M.; Zarkogiannis, S.D.; Antonarakou, A. Integrated Porosity Classification and Quantification Scheme for Enhanced Carbonate Reservoir Quality: Implications from the Miocene Malaysian Carbonates. *J. Mar. Sci. Eng.* **2021**, *9*, 1410. [[CrossRef](#)]
84. Gordon, J.B.; Sanei, H.; Pedersen, P.K. Secondary porosity development in incised valley sandstones from two wells from the Flemish Pass area, offshore Newfoundland. *Mar. Pet. Geol.* **2022**, *140*, 105644. [[CrossRef](#)]
85. Marghani, M.M.; Zairi, M.; Radwan, A.E. Facies analysis, diagenesis, and petrophysical controls on the reservoir quality of the low porosity fluvial sandstone of the Nubian formation, east Sirt Basin, Libya: Insights into the role of fractures in fluid migration, fluid flow, and enhancing the permeability of low porous reservoirs. *Mar. Pet. Geol.* **2023**, *147*, 105986.
86. Khan, A.; Kelling, G.; Umar, M.; Kassi, A. Depositional environments and reservoir assessment of Late Cretaceous sandstones in the south central Kirthar foldbelt, Pakistan. *J. Pet. Geol.* **2002**, *25*, 373–406. [[CrossRef](#)]

**Disclaimer/Publisher's Note:** The statements, opinions and data contained in all publications are solely those of the individual author(s) and contributor(s) and not of MDPI and/or the editor(s). MDPI and/or the editor(s) disclaim responsibility for any injury to people or property resulting from any ideas, methods, instructions or products referred to in the content.